TNO innovation for life

Geochemical characterization of Eocene to Miocene deposits of the DAPGEO-2 borehole in Delft

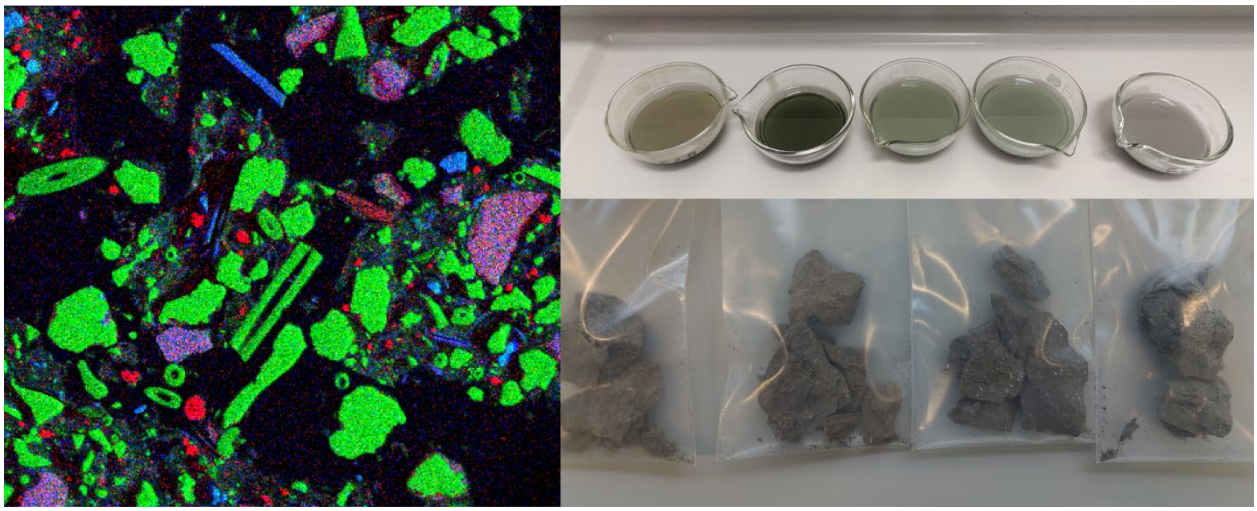

TNO Intern ⟩ TNO 2025 R12729
3 december 2025

Energy & Materials Transition
www.tno.nl
+31 88 866 42 56
info@tno.nl

TNO 2025 R12729 – 3 december 2025

Geochemical characterization of Eocene to Miocene deposits of the DAPGEO-2 borehole in Delft

Author(s)	Alwina Hoving, Jasper Griffioen, Joëlle Kubeneck
Classification report	TNO Intern
Title	TNO Intern
Report text	TNO Intern
Number of pages	39 (excl. front and back cover)
Number of appendices	0
Project name	Geochemische sedimentanalyses – COVRA
Project number	060.59764

Samenvatting/ Summary

Samenvatting

In Nederland wordt berging in ondergrondse, dikke kleilagen overwogen als een van de mogelijke opties voor eindberging van radioactief afval. Kleilagen hebben een lage doorlatendheid en hebben een hoge retentie-capaciteit waardoor zij een goede barrièrefunctie hebben. Inzicht in de geochemische eigenschappen van de kleilagen is nodig om de eigenschappen en geschiktheid te kunnen vaststellen. In het kader van het COPERA 2020-2025 onderzoeksprogramma heeft de TU Delft kernmonsters verzameld uit het kleirijke Paleogeen en Neogeen die werden doorboord bij het boren van het DAPGEO-2-boorgat voor monitoring van de productie van geothermische energie. Als onderdeel van het COPERA 2020-2025 onderzoeksprogramma analyseren we in deze studie de geochemische en mineralogische samenstelling van 20 sedimentmonsters uit het Paleogene en Neogene interval. In deze studie is voornamelijk gekeken naar de Formatie van Diessen, de Groote Heide Formatie en de Formatie van Dongen. De Formatie van Landen is in deze studie niet uitgebreid onderzocht. Naast een algemene karakterisatie worden vijf sporenelementen in meer detail onderzocht. Het uitgangspunt hierbij is dat het geochemische gedrag van een radioactieve element gelijk is aan het gedrag van datzelfde, stabiele element en dat sommige natuurlijk voorkomende, stabiele elementen geochemisch vergelijkbaar gedrag vertonen met radioactieve elementen (''natural analogues''). De nader onderzochte sporenelementen zijn Se, U, Th, Cs en Eu. Bij diepe ondergrondse berging van radioactief afval zijn de belangrijkste chemische retentieprocessen van radionucliden uit afval (co-)precipitatie en adsorptie. De natuurlijke radionucliden en analogen in sediment kunnen worden geadsorbeerd aan mineralen (bijv. kleimineralen) of aanwezig zijn in de structuur van een geprecipiteerd mineraal (bijv. calciet) of detritisch mineraal (bijv. veldspaat, zirkoon). De aanwezigheid van natuurlijke radionucliden in detritische mineralen zal waarschijnlijk geen voorspellende waarde hebben voor het gedrag van radionucliden uit afval, terwijl hun aanwezigheid in geprecipiteerde mineralen of in de geadsorbeerde fractie dat wel zou kunnen hebben.

De mineralogie en geochemische samenstelling zijn bestudeerd aan de hand van bulk-analyses aangevuld met electronenmicroscopie, chemische extracties en laser-ablation-ICP-MS. Het Neogene interval omvat de Diessen Formatie, welke voornamelijk uit siltige kleien bestaat en met de diepte wat zandiger wordt, en de Groote Heide Formatie, die in deze kern bestaat uit glauconietrijke fijne zanden. Het geanalyseerde Paleogene sediment bestaat hier uit de Dongen Formatie, die is onderverdeeld in een klei/silt-rijke Ieper Laagpakket en het zandige Oosteind Laagpakket. De diepste Paleogene Formatie, de Landen Formatie, bestaat uit siltige kleien. Alleen de bovenste monsters in de Diessen Formatie zijn kalkrijk, de rest van de geanalyseerde monsters bevat nagenoeg geen kalk. De mineralogie bestaat hoofdzakelijk uit kwarts, kleimineralen, veldspaten en glauconiet. Ook calciet, pyriet en zware mineralen zoals rutiel en zirkonen waren aanwezig. De natuurlijke analogen U, Th, Cs, Se en Eu hadden gemiddelde gehaltes van: U 4 ± 2 ppm, Th 8 ± 4 ppm, Se 1,5 ± 0,7 ppm, Cs 6 ± 3 ppm en Eu 1 ± 0,4 ppm, wat vergelijkbaar is met andere kleiformaties zoals de Boomse Klei. Al deze elementen, behalve Se, vertoonden een hoge correlatie met het gehalte aan kleimineralen. Als we naar individuele mineralen kijken, bevatten zware mineralen zoals rutiel en zirkoon het hoogste gehalte aan de onderzochte sporenelementen, gevolgd door kleimineralen en veldspaten.

Als we rekening houden met het gehalte aan mineralen aanwezig in het sediment, waren kleimineralen de belangrijkste fractie voor al deze sporenelementen. Pyriet en carbonaten, zoals calciet, speelden geen belangrijke rol in deze sedimenten, omdat ze een laag gehalte aan sporenelementen hadden en over het algemeen weinig voorkwamen.

Deze resultaten van mineraal-associaties van natuurlijke analogen van radionucliden kunnen worden gebruikt voor het voorspellen van de retentie van radionucliden op lange termijn en kunnen helpen bij het valideren van de transportmodellen voor radionucliden die worden gebruikt bij de veiligheidsbeoordeling van eindberging van radioactief afval voor het tijdsbereik van meer dan honderdduizend jaar.

Summary

In the Netherlands, disposal in deep, thick clay layers is considered as one of the potential options for the final disposal of radioactive waste. Clay layers have a low permeability and high retention capacity, which provides them with good barrier functions. Insight into the geochemical properties of the clay layers is necessary to assess their properties and suitability. In the context of the COPERA 2020-2025 research programme, Delft University of Technology collected core samples from the Paleogene and Neogene clay layers that were drilled during the DAPGEO-2 geothermal energy drilling project. As part of the COPERA programme, this study analyzes the geochemical and mineralogical composition of 20 sediment samples from the clay-rich Paleogene and Neogene interval. This study mainly focused on the Diessen Formation, the Groote Heide Formation, and the Dongen Formation. The Landen Formation was not examined in detail. In addition to a general characterization, five trace elements were examined in more detail. The geochemical behavior of a radioactive element is the same as that of the same stable element, and some naturally occurring stable elements exhibit geochemically similar behavior to radioactive elements (“natural analogues”). The trace elements examined in more detail are Se, U, Th, Cs, and Eu.

The mineralogy and geochemical composition were studied using bulk analyses supplemented with electron microscopy, chemical extractions, and laser ablation ICP-MS. The Neogene interval comprises the Diessen Formation, which consists mainly of silty clays and becomes somewhat sandier with depth, and the Groote Heide Formation, which in this core consists of glauconite-rich fine sands. The Paleogene sediment samples analyzed in this study consist of the Dongen Formation, which is subdivided into a clay/silt-rich Ypresian Member and the sandy Oosteind Member. The deepest Paleogene Formation, the Landen Formation, consists of silty clays. Only the uppermost samples of the Diessen Formation are calcareous; the rest of the analyzed samples contain limited amounts of carbonates. The bulk mineralogy consists mainly of quartz, clay minerals, feldspars and glauconite. Calcite, pyrite and heavy minerals such as rutile and zircons were also present in minor to trace quantities. The natural analogues U, Th, Cs, Se, and Eu had average contents of: U 4 ± 2 ppm, Th 8 ± 4 ppm, Se 1.5 ± 0.7 ppm, Cs 6 ± 3 ppm, and Eu 1 ± 0.4 ppm, which is comparable to other clay formations such as the Boom Clay. In deep underground radioactive waste disposal, the most important chemical retention processes of radionuclides from waste are (co-)precipitation and adsorption. The natural radionuclides and analogues in sediment can be adsorbed to minerals (e.g. clay minerals) or present in the structure of a precipitated mineral (e.g. calcite) or a detrital mineral (e.g. feldspars, zircon). The latter source of natural radionuclides (i.e. detrital minerals) will likely not be of predictive value for the behavior of radionuclides from waste, while their presence in precipitated minerals or in the adsorbed fraction could be.

All these elements, except Se, showed a high correlation with clay minerals content. When focusing on individual minerals, heavy minerals such as rutile and zircon contained the highest levels of the trace elements studied, followed by clay minerals and feldspars. When taking into account the mineral content present in the sediment, clay minerals were the most important fraction for all these trace elements. Pyrite and carbonates, such as calcite, did not play an important role in these sediments, as they had low trace element content and were generally present in low quantities.

These results of mineral associations of natural analogues of radionuclides can be used to predict the long-term retention of radionuclides and can help validate the retention models of radionuclides used in the safety assessment of final disposal of radioactive waste.

Contents

1 Introduction

In the context of radioactive waste disposal, thick clay layers are considered as potential option to host a deep underground repository due to their low hydraulic permeability, and in general due to the high sorption capacity of clays. In the Netherlands, Paleogene clay layers could be eligible for this purpose, and therefore geoscientific information of these clays is needed to assess their properties and suitability. In this context, specific research is carried out on these clays which is coordinated by COVRA, the organization responsible for collecting, processing and storing radioactive waste in the Netherlands. This study is performed as part of COVRA's research program COPERA 2020-2025.

In the context of the COPERA 2020-2025 research programme, TU Delft collected core samples from the Paleogene clay layers that were drilled through when the DAPGEO-2 borehole for monitoring the production of geothermal energy was drilled. After analysis, about half of the cored samples appeared to be of Neogene origin (Munsterman, 2023). These clay samples are analyzed extensively in terms of their geomechanical and geochemical properties (DAPGEO-02 Multi-Purpose Research Borehole).

Specific trace elements that exhibit geochemical behavior analogue to radionuclides in waste can be studied to understand and predict long-term radionuclide behavior in the host rock. Such behavior is also studied by laboratory experiments. However, these experiments are relatively short-term compared to the expected migration period of radionuclides released from radioactive waste and it is very challenging to imitate disposal representative conditions in an above ground laboratory. Natural analogue studies can focus directly on radionuclides such as U, or alternatively, on stable isotopes of the same element, for example, Se and Cs. One can also study a different element that behaves chemically in a similar manner, a 'chemical analogue', for example: studying rare earth elements like Eu for trivalent actinides (Am^{III}, Cm^{III}, Pu^{III}, Np^{III}, U^{III}), or Th for Pu^{IV} (De Craen et al., 2000).
In deep underground radioactive waste disposal, the most important chemical retention processes of radionuclides from waste are (co-)precipitation and adsorption. The natural radionuclides and analogues in sediment can be adsorbed to minerals (e.g. clay minerals) or present in the structure of a precipitated mineral (e.g. calcite) or a detrital mineral (e.g. feldspars, zircon). The latter source of natural radionuclides (i.e. detrital minerals) will likely not be of predictive value for the behaviour of radionuclides from waste, while their presence in precipitated minerals or in the adsorbed fraction could be.

In this study, a wide range of geochemical analyses of samples from Eocene to Miocene sediments in the DAPGEO-2 drilling in Delft were conducted, as was commissioned by COVRA. In addition to characterizing the mineralogy and major elemental composition, there is a special focus on specific trace elements, U, Th, Eu, Cs and Se, and their mineral association as a natural analogue to radionuclides.

2 Methods

For this investigation, the Eocene to Miocene deposits of the DAPGEO-2 drilling were investigated. TNO received subsamples of shoe samples from TU Delft from the depth interval 397.7-362.5 m below surface (shoe numbers 19-21, 24-26, 42-44, 48-55, 57, 62). Due to a change in the official sample coding by TU-Delft it was erroneously concluded that some shoe samples were not present, which is why there are no shoe samples from the Landen Clay analyzed. Sample numbers and corresponding depths are listed in Table 2.1. Since the shoe samples had not been protected from air, they were prone to oxidation and drying (Fig. 2.1). The presence of secondary minerals can therefore be expected. In addition, there were three samples from fresh cores (C20, C57, and C75) that are analyzed for their pore water composition (Ma et al., 2025)

Mineralogy was analyzed by X-Ray Diffraction (XRD, Bruker D8 Advance with DAVINCI). For quantitative mineral analysis of the bulk samples, corundum was added as an internal standard and the mixture was ground using a McCrone mill. Clay mineralogy was analyzed using the method described by Zeelmaekers (2011).

Another subsample of the shoe samples was ground in an agate mortar after which it was used for major, minor, and trace elements analysis by X-Ray Fluorescence (XRF, Thermo ARL 9400 sequential XRF). Major elements were measured on a fusion bead while trace elements were measured on a pressed pellet. Total carbon (C_{total}), organic carbon (C_{org}) and total sulfur content were analyzed by combustion and infrared detection (Leco SC632). Thermogravimetric analysis was carried out to assess the organic matter content and carbonate content (Leco TGA701). Not all trace elements of interest can be analyzed by XRF. Therefore the sample was also analyzed by Inductively Coupled Plasma-Mass Spectroscopy (ICP-MS, PerkinElmer NEXION 2000P) after digesting the sediment in an HF-HNO_3-$HClO_4$ solution.

To assess the mineral association of the trace elements, a sequential extraction was carried out on the same subsamples that clay mineralogy was later-on performed on. The sequential extraction consisted of 4 steps targeting 1. Exchangeable ions (1 M $MgCl_2$ solution, 1h), 2. Carbonates and carbonate-bound ions (1 M Na-acetate/acetic acid pH 4.5, 24h), 3. Organic matter (0.7M Na-hypochlorite, 85°C, 3 x 15 min), 4. Fe/Mn-oxides (0.2M oxalate/oxalic acid, 97°C, 30 min) (Gleyzes et al., 2002). The extracts were analyzed by ICP-MS.

In addition, Laser Ablation-ICP-MS was carried out on a few mineralogically very different samples to identify the trace elemental content of different minerals. Samples were chosen based on XRF, inorganic and organic carbon content as well as distribution over the different Formations: a carbonate-rich clayey silt sample (C19), an organic carbon-rich clayey fine sandstone sample (C42), a glauconite-rich fine sandstone sample (C51) and a silt from the Dongen Formation (C55). These samples were embedded in epoxy and polished. The same thin sections were also analyzed with Scanning Electron Microscopy with energy dispersive X-ray spectroscopy (SEM-EDX).

Table 2.1 Depth, geological formation and sample labelling of the samples from core DAPGEO-02 that are studied in this report.

Core sample	Shoe	Core Bottom Depth (m)	Core Top Depth (m)	Geological Formation
DAPGEO-02-C19	SH1	363.4	362.5	Diessen
DAPGEO-02-C20*	SH2	364.1	363.4	Diessen
DAPGEO-02-C21	SH3	364.88	364.1	Diessen
DAPGEO-02-C24	SH4	366.71	365.9	Diessen
DAPGEO-02-C25	SH5	367.71	366.7	Diessen
DAPGEO-02-C26	SH6-2	368.51	367.7	Diessen
DAPGEO-02-C42	SH20	381.1	380.1	Diessen
DAPGEO-02-C43	SH21	382.1	381.1	Diessen
DAPGEO-02-C44	SH22	382.95	382.1	Diessen
DAPGEO-02-C48	SH25	386.05	385.2	Grootte Heide
DAPGEO-02-C49	SH26	386.95	386.1	Grootte Heide
DAPGEO-02-C50	SH27	387.9	387	Grootte Heide
DAPGEO-02-C51	SH28	388.85	387.9	Grootte Heide
DAPGEO-02-C52	SH29	389.69	388.9	Grootte Heide
DAPGEO-02-C53	SH30	390.69	389.7	Dongen (Ieper)
DAPGEO-02-C54	SH31	391.21	390.2	Dongen (Ieper)
DAPGEO-02-C55	SH32	392.21	391.2	Dongen (Ieper)
DAPGEO-02-C57*	SH33	393.66	392.7	Dongen (Ieper)
DAPGEO-02-C62	SH34	397.75	396.9	Dongen (Oosteind)
DAPGEO-02-C75*		405.11	406.11	Landen (Liessel)

*These depth intervals had both a shoe sample and fresh core material analyzed, or only fresh core material (C75).

Figure 2.1. Left: bags with subsamples of shoe samples from DAPGEO-02 as received from TU Delft. Right: Centrifuge tubes with samples during the sequential extraction.

3 Results

3.1 Major elements and main mineralogy

The core descriptions of the shoe samples analyzed for this study are presented in appendix A. In Fig. 3.1, a depth profile of major elements is plotted together with lithology and mineralogy. The samples from the top of our interval, belonging to the Diessen Formation, are described as silty clay, while the deeper parts of our interval, which are identified as Diessen, Grootte Heide and Dongen Formation, predominantly consist of very fine sand. The quartz content fluctuates with depth having higher values at the sandier intervals and lower values at the clayey intervals, with the sample from the Oosteind Formation having the highest content of 93 wt%. The clayey intervals coincide with samples having the highest aluminium content. Alumium (Al) is a major element in clay minerals, but also in feldspars. The feldspar content is quite constant throughout the depth profile with values around 7 ± 2 wt%. Only the deepest sample, C62 at 397 m depth, has a much lower feldspar content of around 1.5 wt%. The Ca content correlates well with calcite and is highest in the interval between 362 and 368 m depth with an average content of 5 wt% calcite. The interval between 385 and 389 m depth has a high iron (Fe) content (C48-C52, 6.6-8.8 wt%). This interval is described as glauconitic fine sand which likely explains the increased Fe content since glauconite can be iron-rich. The sulfur (S) content correlates well to the pyrite (FeS_2) content and fluctuates throughout the depth profile. Organic carbon content also fluctuates with depth. Both sulfur and organic carbon lack a clear correlation to lithology or any of the other major elements.

The mineralogy of the bulk samples is listed in Table 3-1. The main constituents of these samples are quartz, phyllosilicates (2:1 clay minerals, micas and glauconite which are difficult to distinguish from each other in XRD of bulk samples), feldspars, calcite and kaolinite. The content of each of these minerals varies greatly, which is caused by the fact that the analyzed samples contain both clays and sandstones. In addition to these main constituents, low quantities (on average <1%) were present of ankerite, siderite, pyrite, rutile and anatase. Jarosite and gypsum were also present with maximum quantities of 3% and 5%, respectively. These secondary minerals can form upon oxidation of the sediment and evaporation of the pore water. In sediments containing pyrite and carbonates such as calcite, oxidation can lead to the formation of gypsum and Fe-(oxyhydr)oxides. Oxidation of pyrite releases acidity which results in the dissolution of carbonates. If all carbonates are dissolved, the pH decreases and jarosite can form as an oxidation product. Assuming all S originates from pyrite, the original pyrite content of these sediments would have been on average 2.2 ± 1.3%.

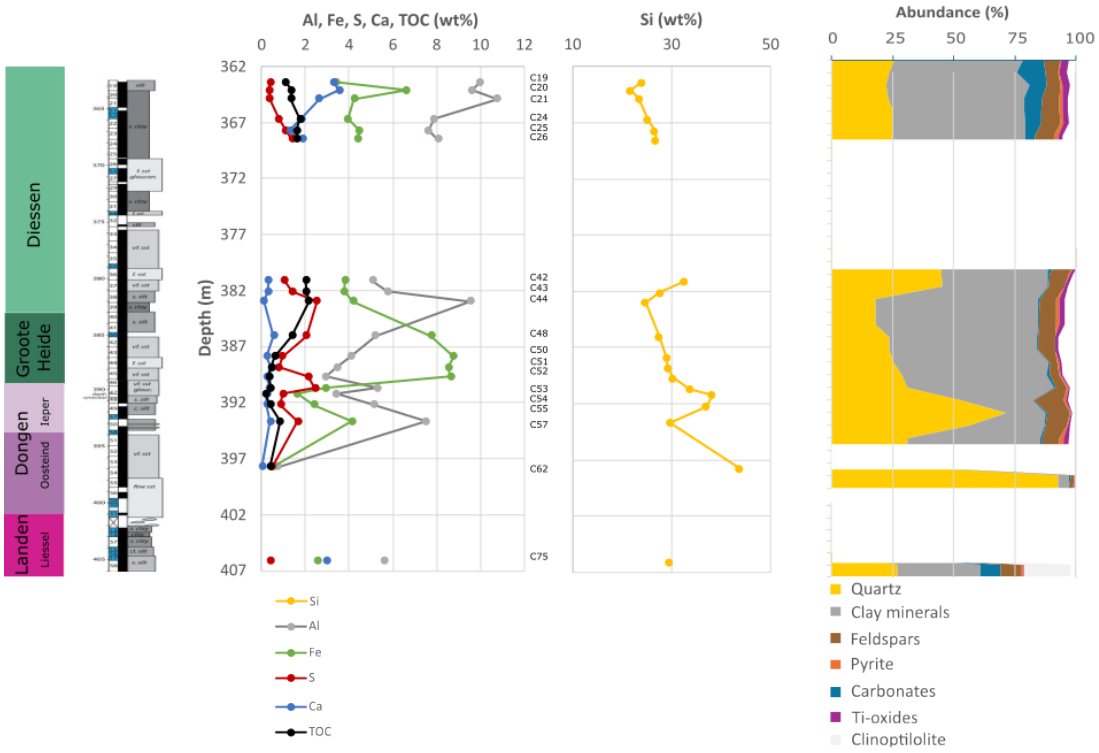

Figure 3.1: Depth profile of the analyzed depth interval of core DAPGEO-02 with main lithology (left), total inorganic carbon (TIC), organic carbon (TOC), aluminium (Al), iron (Fe), and silicium (Si) content (middle), and main mineralogy (right). In the mineralogy graph 'clay minerals' include micas and glauconite.

Table 3-1: Summary of the mineralogy of the DAPGEO-02 samples from the depth interval 362-397 m below surface.

Mineral	MIN (wt%)	MAX (wt%)	Median (wt%)
Quartz	18	93	27
Phyllosilicates (2:1 clay minerals/ micas/ glauconite)*	4	61	51
Illite/mica	1	23	15
smectite	3	38	24
Kaolinite	0	19	7
Chlorite	0	3	0.3
Feldspars	2	12	7
Calcite	0	9	2
Ankerite	0	5	1
Pyrite	0	2	1
Rutile	0	1	1
Anatase	0	2	1
Gypsum	0	5	2
Jarosite	0	3	1

*The peaks of clay mineral illite, micas (e.g. muscovite and biotite) and glauconite are located at similar 2theta angles and are therefore hard to distinguish in bulk XRD analysis. In italic, the illitic and smectite content obtained from XRD of the clay fraction

3.2 Clay mineralogy

The relative quantities of the various clay minerals vary with depth (Fig. 3.2). Interstratified illite/smectite (I-S) and smectite were most abundant in all samples with values between 20-40% and 20-60% of the <2 µm size fraction, respectively. The smectitic content (smectite content + smectitic layers in I-S) of the <2 µm size fraction increased with depth, with the lowest content at the top of the Diessen Formation and the highest content in the Dongen Formation. The opposite holds for the illitic content and the kaolinite content, which were on average higher in the Diessen Formation and lower in the Dongen Formation. An exception is the kaolinite peak at 382 m depth. Chlorite was least abundant with values between 0 and 4% of the <2 µm size fraction.

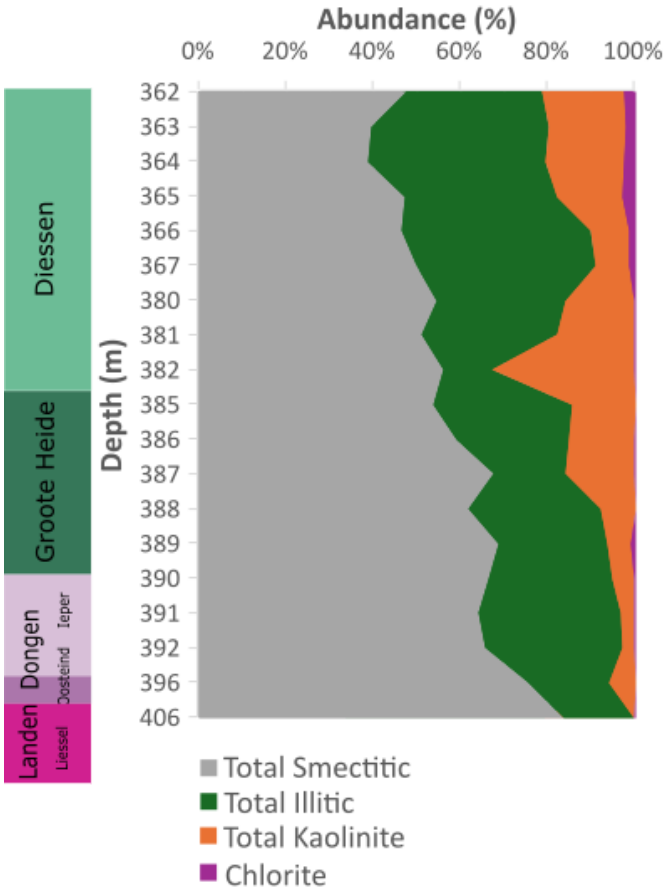

Figure 3.2 Relative clay mineralogy of the <2 µm size fraction. Smectitic content refers to the sum of smectite and smectitic layers in interstratified illite/smectite (I-S), and the illitic content refers to the sum of illite and illitic layers in interstratified illite/smectite (I-S).

3.3 SEM imaging

Scanning Electron Microscopy (SEM) imaging combined with EDX (Energy Dispersive X-ray Spectroscopy) was performed on samples C19, C42, C51 and C55 (Fig. 3.3). An example of an element map using EDX is shown in Fig. 3.4. The main focus of the SEM analysis was to characterize the minerals in which the naturally occurring radionuclides, or natural analogues for radionuclides, are expected to be present. Feldspars, clay minerals, carbonates, pyrite, glauconite, micas, titanium-oxides and heavy minerals such as zircon and monazite, were analyzed by EDX for their elemental content. These results were used for the quantification of trace elements on the same spots by LA-ICP-MS. Most heavy minerals were present in trace quantities that are below the detection limit of the XRD analysis, for which reason their bulk content could not be determined. General chemical formulas of these minerals are listed in table 3.2.

All samples contained varying abundances of quartz, feldspars, micas and clay minerals. The micas contained Mg and Fe and therefore classify as biotite. Sample C19 was clay minerals rich and pyrite framboids were abundant. Additionally, there were many carbonate shell fragments in this sample. Sample C42 was quartz- and mica-rich and contained many siliceous fossils and some glauconite grains. In addition, there were also zircons and monazites. Monazite is a phosphate mineral which is very enriched in rare-earth elements (REEs) like cerium and lanthanum, as well as thorium. In sample C51, glauconite was very abundant and in addition to pyrite framboids there was also ilmenite ($FeTiO_3$) present. Sample C55 contained both euhedral and framboidal pyrite. Heavy minerals, such as titanium-oxides and zircon, were also present in this sample.

Table 3-2: List of minerals present in the analyzed samples and their general structural formulas. The minerals zircon to monazite are also known as 'heavy minerals'.

Mineral	Chemical formula
Plagioclase (Na-Ca-feldspar)	$Na_{1-x}Ca_xAl_{1+x}Si_3{-}xO_8$
K-feldspar	$KAlSi_3O_8$
Glauconite	$K_{0.60\text{-}0.85}(Fe^{3+},Mg,Al)_2(Si,Al)_4O_{10}](OH)_2$
Biotite (mica)	$K(Mg,Fe)_3AlSi_3O_{10}(F,OH)_2$
Pyrite	FeS
Zircon	$ZrSiO_4$
Ilmenite	$FeTiO_3$
Rutile/anatase	TiO_2
Sphene/titanite	$CaTiSiO_5$
Monazite	$(Ce,La,Y,Th)PO_4$

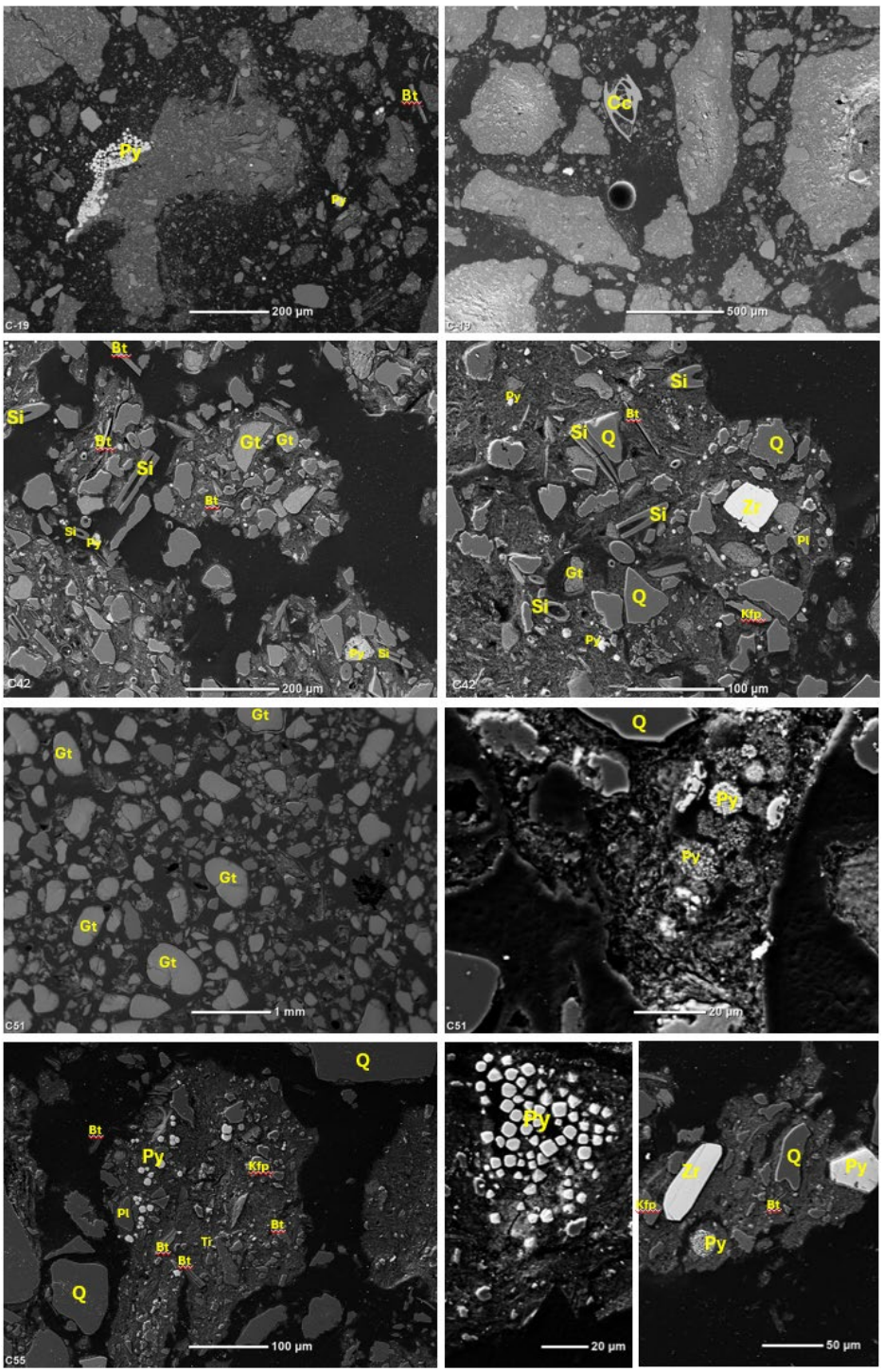

Figure 3.3: Backscatter-electron Scanning Electron Microscope (BSE-SEM) images of samples C19, C42, C51 and C55. A few characteristic minerals are indicated with Q = quartz, Gt = glauconite, Bt = biotite, Kfp = K-feldspar, Pl = plagioclase, Py = pyrite, Ti = titanium oxide mineral, Cc = calcite, Si = SiO_2-fossils, Zr = zircon. The white grains contain heavier atoms and represent e.g. pyrite , Ti-oxides and zircon. All micrometer-sized, medium-grey particles in between the larger grains are clay minerals.

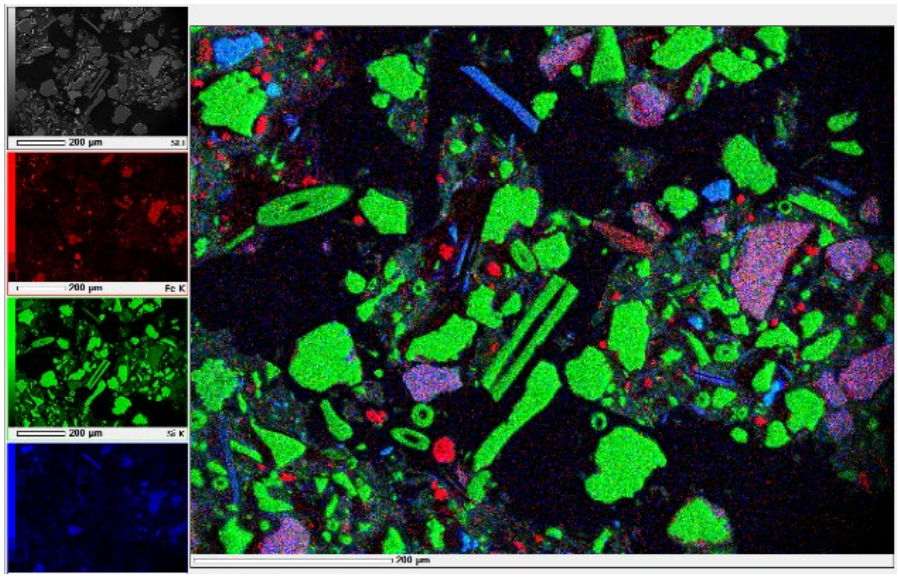

Figure 3.4. Example of SEM-EDX elemental mapping of sample C42 for Si (green), Fe (red) and K (blue). The green particles are clearly identified as silica microfossils and quartz grains, the purple colors are glauconite grains, the blue colors are micas (thin grains) and K-feldspars, and the red colored small grains are pyrite grains.

3.4 Trace elements

3.4.1 Trace element content

The trace elemental content of all the samples is presented in Appendix D. Results of a few relevant trace elements that can be used as natural analogue for radionuclides in radioactive waste will be described in this section. The uranium content was on average 4.4 ± 2.0 ppm, Th 8.1 ± 3.9 ppm, Se 1.5 ± 0.7 ppm, Cs 6.1 ± 3.0 ppm, Eu 1.0 ± 0.4 ppm and Re 13 ± 10 ppb. Depth profiles of U, Th and Cs are plotted in Fig. 3.5. The Th and Cs content is on average highest in the Diessen Formation compared to the Groote Heide and Dongen Formations. They follow the same trend as Al. The good correlation between Th and Al is also visible in Fig.3.6. The U content peaks at 385 m depth which coincides with a peak in phosphorous content at that depth. The Groote Heide Formation (part of the former Breda Fm) is known to contain phosphorites that are rich in uranium (Balson, 1989; Harsveld, 1973; Meijer et al., 2016). Selenium and Eu show similar depth profiles as Th and Cs, although Se has its highest peak at 385 m depth, similar to U.

To find out to which phase the trace elements are associated, correlations between trace elements and major elements or minerals can be investigated. A correlation matrix was created between the measured trace and major elements (Appendix B). This matrix displays the linear correlation coefficients between multiple variables, showing how strongly pairs of variables are related. In table 3-3, the parameters with correlation coefficients higher than 0.7 are grouped together. A separate correlation matrix with main mineralogy and major elements Si, Al, Ca, Ti, S and trace elements U, Th, Cs, Ce and Pb was calculated (Appendix C).

Trace elements Th, Cs, and rare earth elements (REE) correlate well to the Al content (group 1 in Table 3-3) and to clay minerals (group B in Table 3-4). They also correlate well with the Ti-oxide anatase (group D). Thorium also correlates well to feldspars (group A).
Group 2 in Table 3-3 contains Fe, K, Mg and Be and likely represents glauconite or biotite which are both rich in these elements.

Chromium is well-known to be able to substitute Fe in Fe-bearing minerals (e.g. Schwertmann et al., 1989; Oze et al., 2019). Beryllium concentrations have been mentioned to be elevated in glauconite (Dooley, 2001). Group 3 and 4 represent zircon and calcite, respectively. These groups had no natural analogue trace elements correlated to them. The last group contains Cd, Se, Re and U and lacks any major elements and therefore has no clear mineralogy related to them. These elements are also often related to organic matter (Stockdale and Brian, 2013; Zhang et al., 2024; Gustafsson and Johnsson, 1992). Sulfur (S), the main element in pyrite, does not show good correlations to any of the trace elements.

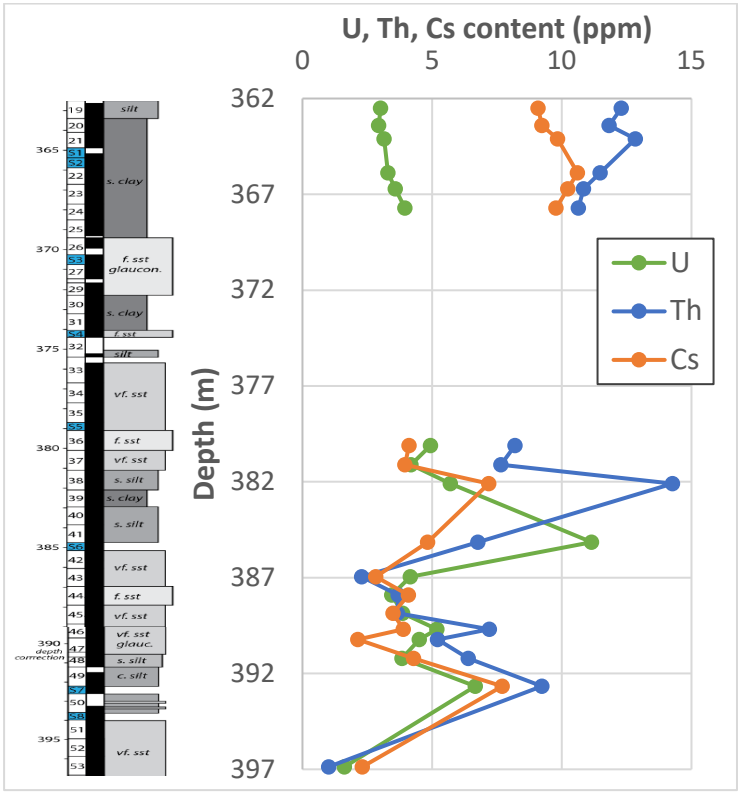

Figure 3.5. Depth profiles of uranium (U), thorium (Th) and cesium (Cs) content in sediment of the DAPGEO-02 borehole..

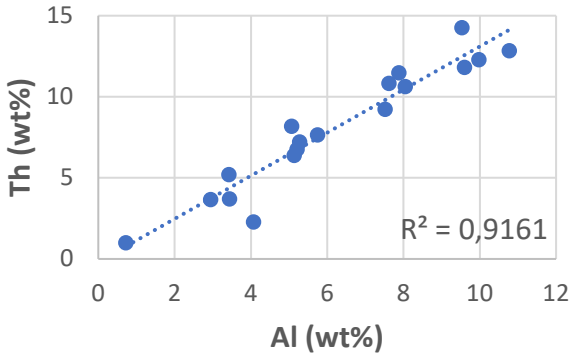

Figure 3.6. The thorium content versus aluminium content in the analyzed DAPGEO-02 samples showing the good correlation between them.

Table 3-3. Elemental groups having high correlation coefficients ($R^2 > 0.7$) that are recognized from the correlation matrix presented in Appendix B. Elements in blue are trace elements that can be a natural analogue for radionuclides. The third column lists minerals that could potentially represent the groups of elements, based on the chemical formulas of these minerals.

Group	Elements in group	Potentially associated minerals
Group 1	Al, Ti, Ba, Cu, Pb, Ga, Nb, V, Li, Ta, Ni, LREE, HREE, Th, Cs.	Phyllosilicates (clay minerals/micas), feldspars, Ti-oxides
Group 2	Fe, K, Mg, Cr, Be	Glauconite/Biotite
Group 3	Zr, Hf, Ag	Zircon
Group 4	Ca, TIC, Mn	Calcite
Group 5	Cd, Se, Re, U	-

Table 3-4. Groups of minerals and elements with high correlation coefficients ($R^2 > 0.7$). Elements in blue are trace elements that can be a natural analogue for radionuclides.

Group	Correlated parameters (R^2>0.7)
Group A	Feldspars: Al , Ti, Ba, Th
Group B	Clay minerals/Mica: Cs, Ce, Th
Group C	Calcite: Mn
Group D	Anatase: Ce, Nd, Th, Cs

3.4.2 Mineral specific trace elemental content

3.4.2.1 Results sequential extraction

The sequential extraction targets different mineral groups and solid organic matter in the sediment to evaluate the trace elemental content associated to them. The extraction scheme used in this study does not include the residual fraction, since it is not mineral specific because it will dissolve feldspars, glauconite, heavy minerals and clay minerals. These minerals are analyzed by LA-ICP-MS and will be discussed in the next section. The extraction results of a few characteristic samples are discussed here.

In general, the extracted trace element content for the various extraction steps was very different between different samples and for different elements (Fig. 3.7). The first extraction step targets exchangeable ions that are electrostatically adsorbed to clay minerals or organic matter. Th and Cs are not extracted in step 1, while U, Eu and Se are. Cs is known to be affiliated to the clay phase (Fuller et al., 2015); therefore Cs would be expected to be released in the first extraction step. Its absence could be explained by the high affinity of Cs to (illitic) clay minerals and the associated difficulty of desorption in extraction methods (Herr et al., 2022; De Koning and Comans, 2004).

Sample C51 had the highest adsorbed content of Eu, Se and U (Av. 175 ± 45 µg/kg sample), followed by sample C62 (Av. 110 ± 106 µg/kg sample) and sample C19 (Av. 16 ± 14 µg/kg sample). The second extraction step targeting carbonates, such as calcite, and carbonate-bound ions, mainly contained U (Av. 470 ± 156 µg/kg). Sample C48 had an extremely high U content (1860 µg/kg) compared to the other samples. This sample also had a high bulk U content coinciding with a high P content. The sediments from the Groote Heide Formation are known to contain phosphorites, often consisting of apatite, that contain high amounts of U. Possibly some of the apatite dissolved or preferentially extracted U from the apatite in this extraction step. In addition, Th (112 ± 86 µg/kg) and Se (64 ± 30 µg/kg) were also extracted and for sample C19, also Eu. In the third step which extracts organic matter, the Se content (124 ± 67 µg/kg) and U content (140 ± 60 µg/kg) were highest of the five trace elements discussed here. Th was extracted predominantly in the oxalate step (513 ± 360 µg/kg) which extract Fe-, Al- and Mn-oxides. The original sediment of this borehole consisted of reduced sediments. In the fresh core material, no Fe-oxides were visible. However, the oxic storage of these shoe samples resulted in the formation of Fe-oxy(hydr)oxides. U, Th and Se are known to adsorb to Fe-(oxyhydr)oxides (Ithurbide, 2009; Su and Suarez, 2000; Reiller et al., 2002). The sequential extraction of the fresh core material resulted in lower extracted Fe in step 3 compared to the average Fe extracted in step 3 of the shoe samples, also resulting in lower extracted U, Th and Se. Extraction step 2 of the core material gave results of the same order of magnitude to those of the shoe samples, while step 3, targeting organic matter resulted on average a slightly higher U content compared to the shoe samples.

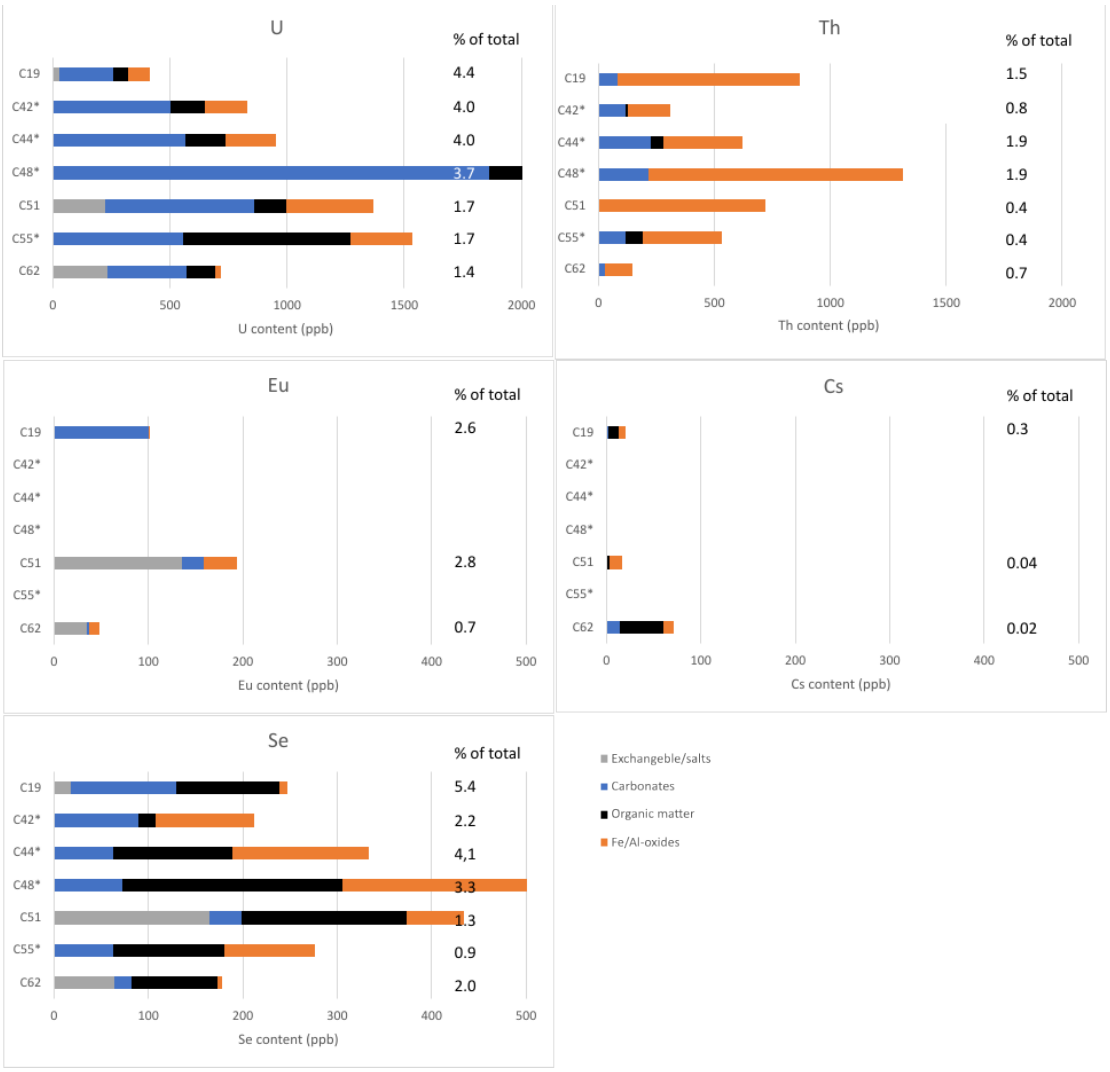

Figure 3.7. Sequential extraction results; uranium, thorium, europium, cesium and selenium content in various fractions. The '% of total' indicates the percentage of the element extracted in all 4 steps with respect to the total amount of this element present in the sample as measured by XRF/ICP-MS. Samples indicated with a * have been analysed by TXRF due to the unavailability of the ICP-MS. This method was not able to measure Eu and Cs since they were below the detection limit, and the $MgCl_2$ extract had to be diluted substantially which also resulted in values below detection limit and the absence of results for the exchangeable/salt fraction.

3.4.2.2 Laser-ablation-ICP-MS

Results from laser-ablation-ICP-MS are plotted in Fig 3.8. The heavy minerals monazite and zircon, and to a lesser extent the titanium minerals, contained the highest content of U and Th with values up to 340 mg/kg and 1000 mg/kg, respectively. The Th content was also high in feldspars (40 mg/kg) and clay minerals (20 mg/kg). The Eu content was very high in monazite (200 mg/kg) while the other heavy minerals, feldspars and clay minerals had a content of on average 4 mg/kg. For Cs, clay minerals, feldspars, rutile and zircon contained the highest amounts (22 mg/kg). Calcite and pyrite had low contents with respect to these four trace elements.

Even though the trace element content in heavy minerals was very high, the overall contribution to the total content in the sample is less significant since heavy minerals are only present in trace quantities (Fig 3.8).

When taking into account the content of each mineral in the bulk sediment, the main reservoir of U, Th, Eu and Cs was the clay minerals (55-72% of total U/Eu/Th/Cs was present in clay minerals). Feldspars, micas and glauconite contribute to around 20-30% to the total budget of each of these trace elements. For U, the heavy minerals are an important carrier despite their low content, with 20% of total U being present in these minerals.

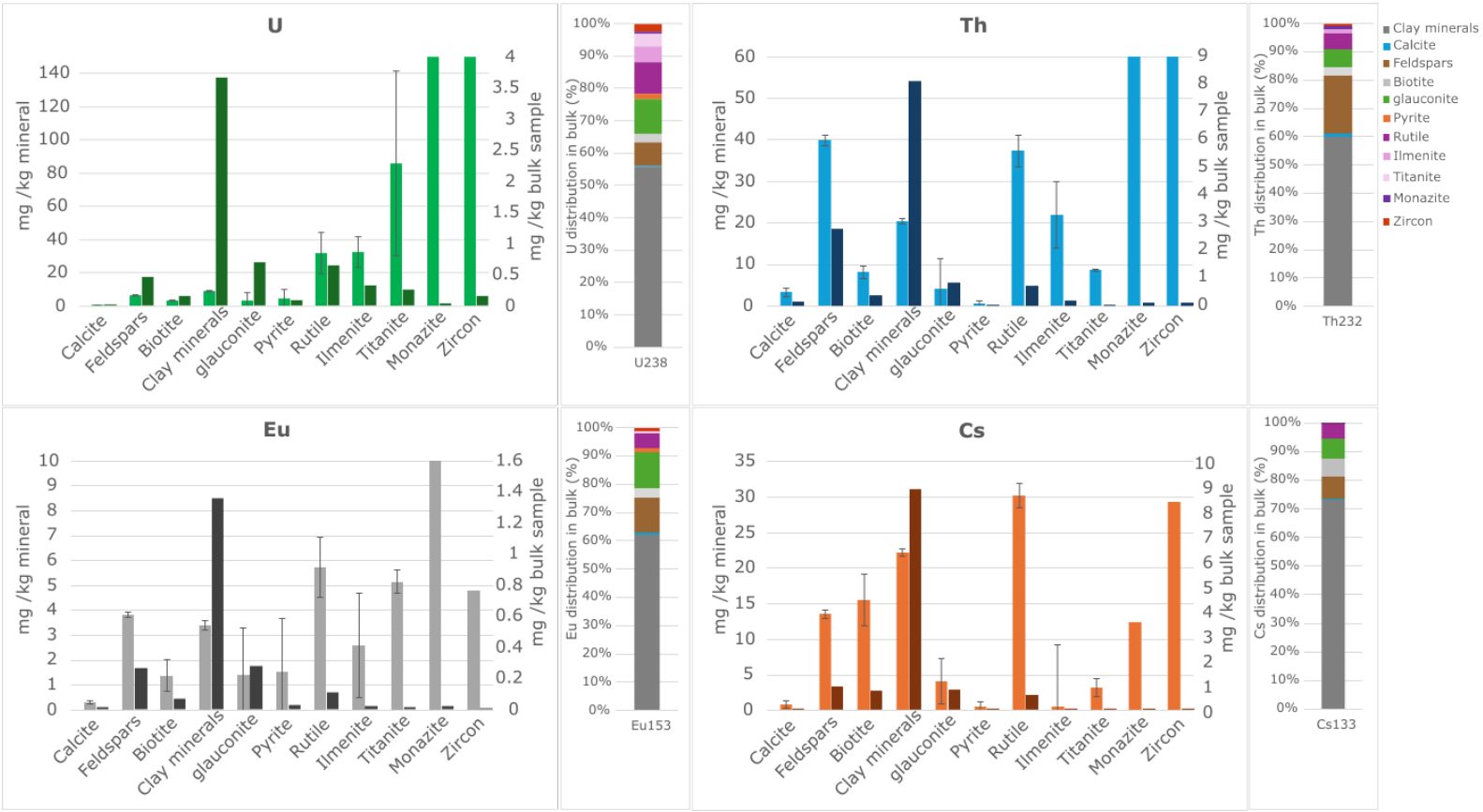

Figure 3.8. The bars in light colors represent uranium, thorium, europium and cesium content in various minerals as measured by LA-ICP-MS in samples C19, C42, C51 and C55. Their values are plotted on the left Y-axis. The detection limit of Se was high, and the results all fell below the detection limit. The darker colored bars show the respective element content recalculated in mg/kg bulk sample (plotted on the right Y-axis). For this, the average values of the mineral content in the four samples were used. The zircon content was based on the Zr content, and the monazite content was set to 0.001 wt%. Glauconite content was taken from XRD (De Jong et al., 2024) and the biotite content was estimated from the difference between total phyllosilicates (minus glauconite) and the clay-size content (De Jong et al., 2024). Error bars represent the standard deviation of the multiple spots measured (10-20 spots per mineral except calcite, ilmenite, titanite, monazite and zircon which had <5 spots). The multi-colored bar on the right side of each graph shows the mineral distribution of each element in the bulk sediment.

4 Geochemical interpretation and discussion

4.1 Mineralogical variations between the different geological formations

In the Netherlands, Paleogene and Neogene clays are of interest to radioactive waste disposal due to their suitable depth, thickness, low permeability, and generally due to the high sorption capacity of clays. Laboratory studies on radionuclides with the Paleogene Boom Clay from Belgium and the Netherlands have concluded that the most important constituents that contributed to the retention of radionuclides, U, Tc, Cs, Se and Am were clay minerals, pyrite, and organic matter (De Canniere et al., 2010; Maes et al., 2008, Hoving et al., 2019, Bruggeman et al., 2017). Also the carbonate system is of importance to the retention of certain radionuclides, such as uranium. On the one hand, high bicarbonate concentrations in solution cause less retention by the formation of U-bicarbonate complexes, while on the other hand precipitation of carbonates can result in coprecipitation of uranium.

Of our analysed samples, the Diessen Formation is the only formation lithologically described as a clay, having the highest clay-size fraction content of 60% (SECUUR report, 2024) and a related high content of clay minerals (XRD). At the top of this Formation is also the highest carbonate content of the samples measured in this study. The fine sands of the Groote Heide Formation are characterized by their glauconite content and the presence of phosphorite at the top. The Dongen Formation has alternating silty and clayey intervals. Pyrite and organic matter content fluctuate throughout the depth interval.
The clay mineralogy of the Dongen Formation had a larger fractions of smectite while the Diessen Formation had the lowest smectite content. The chlorite content was highest in the Diessen Formation. This shift in clay mineral assemblage with depth has been attributed to a change in provenance (Kuhlmann et al. 2004; Zeelmaekers, 2011 ; Nielsen et al., 2015). During the Eocene major extrusive volcanism occurred in the Norwegian Sea (Abdelmalak et al., 2016; Horni et al., 2017) which is represented by tuffaceous, smectite-rich sediments in the Netherlands in the Dongen Formation. From Oligocene towards Miocene and Pliocene time, climatic cooling took place. During the early Miocene times, when the Groote Heide Formation was deposited, the Netherlands was a warm, sub-tropical sea in which glauconites were formed (Munsterman et al., 2025). The climatic changes influenced the source of the sediment in the Netherlands. During colder periods, glacier activity and glacial erosion increased in Scandinavia and sediments were transported over a long distance towards the North Sea bringing in illite- kaolinite- and chlorite-rich clays from the Scandinavian Shield. During warmer climate conditions, smectite-rich sediments derived from more proximal volcanic areas of the southern continent were deposited by enhanced river runoff due to higher precipitation (Kuhlmann et al. 2004).
A different clay mineralogy affects the geochemical and other properties of a Formation. For example, smectite is known for its swelling properties and can be important for a clay's self-sealing properties (Giot et al., 2019). Another property related to clay minerals (and also organic matter) is the cation exchange capacity (CEC).

A higher CEC could result in more adsorption of cationic radionuclides. Samples from the Diessen Formation had similar CEC as samples in the Groote Heide Formation even though their clay content was much higher (De Jong et al., 2024). This could be a result of the different clay mineralogy since illite has a much lower CEC than smectite (Yong et al., 2012).

4.2 Distribution of natural radionuclides and analogues

Non-radioactive counterparts of radionuclides in the waste can be naturally present in sediments as trace elements. Their content can be similar to the content of long-lived radionuclides in the waste forms and, therefore, could provide insights in long-term retention processes of the radionuclides. The trace elements used as analogue in this study are: rare earth elements (REE), such as Eu, for trivalent actinides (Am(III), Cm(III), Pu(III), Np(III), U(III)), Th for Pu(IV), and stable Se, Cs, U for their radioactive counterparts. In radioactive waste modelling there are two dominant chemical retention processes: (co-)precipitation and adsorption. In the first process the radionuclide will be built in the crystal structure of the mineral (e.g. calcite) while in the second process the radionuclides are bound to the surface of a solid (e.g. clay minerals or organic matter). This surface bond can be by either electrostatic forces, forming outer-sphere complexes, or by forming a direct bond to the mineral surface (inner-sphere complexes). In the natural sediment trace elements are also found in detrital minerals that originate from the melt of an igneous source and the weathering thereafter. These minerals are resistant and are transported over large distances. This source of trace elements will not be of predictive value for the behaviour of radionuclides from waste, while their presence in precipitated minerals or in the adsorbed fraction could be, depending on the sufficient availability of components to form (co-)precipitates, and/or the reactivity and amount of sorbents.

The different methods that were used in this study to characterize and analyze the trace element mineral associations mutually strengthen each other. Clay minerals were the most important reservoir for U, Th, Cs and Eu. Feldspars and heavy minerals were also important reservoirs for these trace elements. For Se and U, organic matter was also an important source. It is not entirely clear from these methods whether the trace elements associated with clay minerals are present in the structure of the clay minerals or adsorbed onto their surface. Eu, U and Se were present in the first extraction step representing exchangeable ions but Cs and Th were not. The 1 M $MgCl_2$ extraction step does not desorb adsorbed radionuclides with high affinity to clay minerals such as Cs (Durrant et al., 2018) or radionuclides that are adsorbed through inner-sphere complexation (Chisholm-Brause et al., 2004; Singer et al., 2009). The Al- and Fe-oxide extraction step contained a relatively high concentration of Th, U and Se. The originally reduced sediments likely did not contain Fe-oxyhydroxides as was seen in a study of the well-preserved cores (De Jong et al., 2024, Ma et al., 2025). However, unlike the well-preserved cores, the shoe samples were exposed to air where oxidation and also drying have occurred. This was also observed from the presence of secondary minerals like gypsum and jarosite. The exposure to air likely resulted in oxidation of pyrite resulting in the formation of Fe-oxyhydroxides. The oxidation of pyrite also induces a release of acidity, potentially causing a pH decrease. This could lead to decreased sorption of cations from clay minerals and increased sorption of anionic compounds to these neoformed oxides, (e.g., Dzombak and Morel, 1990).

Two actinides are naturally present in clays: thorium and uranium. They were mostly associated with clay minerals and feldspars. Heavy minerals were also a large source of U. Uranium and thorium in marine sediments originate from various sources (Adams and Weaver, 1958). Organic matter and other reductants in the marine environment reduce uranyl (UO_2^{2+}) dissolved in seawater to tetravalent uranium, which in turn can be fixed in organic complexes or adsorbed on organic material, and clay minerals. This uranium is exchangeable. U and Th also adsorb well onto Fe- and Al- (hydr)oxides. Carbonates that originate from precipitation in a seawater environment, have uranium present in seawater coprecipitated into their structure. Since the carbonate content was rather low in the sediments of the DAPGEO-02 core, this was not a significant reservoir for U.
Next, there are common detrital minerals, such as feldspars, micas and clay minerals that have trace amounts of Th and U present within their structure. Most Th and U in our samples are present in this form as was concluded from the LA-ICP-MS results combined with bulk mineralogy. Clay minerals were the predominant reservoir due to the high content in these samples. For Th, feldspars were also a significant reservoir (20% of total Th). The last group is heavy minerals, such as zircons, monazite, xenotime, apatite and rutile that contain high amounts of Th, U (e.g. Zhu and O'Nions, 1999). These heavy minerals are very resistant to weathering. Even though they are accessory minerals, meaning that they are present in very low contents, their highly enriched trace element content resulted in a contribution of 10-20% of the total Th and U budget. In addition to being an accessory mineral from igneous source rocks, apatite, and more specifically hydroxy-apatite can form through biological processes, being the mineral of which bones consist. Hydroxy-apatite is an effective scavenging phase for U from seawater and therefore can also be enriched in U. This is for example the case in the so called phosphorites from the Breda Formation (Balson 1989) (which is now split-up in the Diessen and Groote Heide Formation) and could be the case in sample C48, although there was no hydroxy-apatite peak visible subsample of C48 used for XRD.

Europium was predominantly present adsorbed to and in clay minerals. The origin of REE's in marine sediments can be similar to what was described for U. They are present as trace elements in seawater from which they can be adsorbed to clay minerals and organic matter and incorporated in carbonates (De Baar et al., 1999). REE's are also present in feldspars and are enriched in heavy minerals, in particular monazite.

Cesium has a strong affinity for clay minerals, in particular illite (Francis and Brinkley 1976). Micas enrich Cs in their structure (Tischendorf et al. 2001). This is also evident from the LA-ICP-MS results which show that clay minerals account for at least 75% of all Cs (Fig 3.8).

Aqueous selenium is often present as the anion selenite or selenate which are not electrostatically attracted to the negatively charged clay minerals. It can form inner-complexes with clay minerals (Missana et al., 2009). Other solid phases to which selenite can adsorb are Fe-, Mn, and Al-(oxy)hydroxides. More reduced forms of Se, can also be retarded by precipitation reactions (e.g. Séby et al., 1998). This is particularly true for Se(-II) in presence of iron(II) and sulfides. The Se content was below the detection limit of the LA-ICP-MS and therefore its content in specific minerals could not be evaluated. The correlation study did not show any correlations with the minerals present. The sequential extraction indicated that Se was associated with organic matter and with Fe-(oxyhydr)oxides which corresponds to what has been found in previous studies (Zhang et al., 2024; Séby et al., 1998; Sharma et al., 2015). However, in the extraction only 5% of total Se was extracted.

In experiments with selenite added to potential host rock clays Callovo-Oxfordian Clay and Belgian Boom Clay they found that the reducing minerals in the sediment resulted in formation of solid elemental selenium (Se^0) (Wang, 2022; Breynaert et al., 2010). Whether reduced solid forms of Se, such as Se^0 or FeSe are present in samples of this study is still an open question.

A similar study, characterizing the natural distribution of U and Eu, was carried out on Callovo-Oxfordian Clay (COx Clay, Montavon et al. 2022; Loni et al., 2021). This clay is a much older (Middle/Upper Jurassic) and more indurated rock that serves as host rock for radioactive waste in France. Despite its different age it is also of marine origin and has a comparable mineralogy (Jacops et al., 2017). They identified the clay minerals to be main mineralogical reservoir for U. Phosphate minerals in their samples contained on average ten times more uranium than clay minerals i.e. 2.5 mg kg^{-1} in clay minerals and 32 mg kg^{-1} in phosphate nodules. Our samples had on average a higher U content in clay minerals of 9 mg/kg clay mineral. The U content in carbonates in our samples (0.6 mg/kg carbonate) was similar to that in COx Clay (0.4-1 mg/kg calcite). The uranium content in organic matter was 0.07 mg/kg in COx while in this study there was a high variation from 0.06 to 1 mg/kg. The U content in pyrite (0.013 ± 0.004 mg kg−1) was very low in COx, while it was higher in our samples, although highly variable (4.9 ± 5 mg/kg).
Europium in COx clay was mainly present in the clay fraction (1.2 ± 0.5 mg/kg of clay fraction) but was also present in the less abundant calcite (0.33 ± 0.15 mg/kg of calcite). Our samples had a slightly higher Eu content in clay minerals (3.4 ± 0.2 mg/kg of clay fraction) and very similar Eu content in calcite (0.3 ± 0.07 mg/kg of calcite).
A correlation study between trace elements and mineralogy was carried out for the Boom Clay in Belgium (De Craen et al., 2000) and the Netherlands (Koenen and Griffioen, 2016). Both studies found that Th, Cs and REE content correlated with clay mineral content. For the Boom Clay, U was correlated with pyrite and organic matter. In our samples pyrite did not have a high correlation with U. In Belgium, U also correlated with apatite and calcite. In the analyzed Dongen and Neogene samples, no clear correlation was evident, but individual samples did show high U and P content. Se in Boom Clay was found to be enriched in pyrite (21.6 ± 7.9 mg kg^{-1}) (De Cannière et al., 2010), which was not found in the samples of this study.

The fact that naturally-occurring elements relevant for radioactive waste disposal such as U, Se, and REE, are concentrated in clay minerals can be useful in the prediction of retention of radionuclides in the long-term. When combining the values obtained in this study with the trace elemental composition of the pore water, which is investigated by Ma et al. (expected in 2025), sorption parameters, such as Kd-values, can be derived that can be used to validate the experiments and predictive models used for radioactive waste disposal studies.

5 Conclusions

A geochemical study was performed on the composition of samples from the Neogene Groote Heide and Diessen Formations and the Paleogene Dongen Formation as obtained from the DAPGEO-02 core. In addition to bulk analyses, mineral specific analysis were performed to analyze their trace elemental content.

The Diessen Formation consisted of clay-rich sediment at the top and became more sandy at greater depths ending again in a clay. The Groote Heide Formation was characterized by glauconitic sands and silts and the Dongen Formation had alternating silty and clayey layers ending in a sand (Dongen Fm Oosteind member). The top of the Diessen Formation had a higher carbonate content (5 wt%), while this is low to zero at greater depths. The main minerals were quartz, clay minerals, glauconite, feldspars and calcite. Pyrite and heavy minerals such as rutile and zircons were also present.

To better understand radionuclide behavior in the context of radioactive waste disposal, naturally-occurring elements/radionuclides with analogue geochemical behavior to radionuclides in waste were studied. In this study, U, Th, Cs, Se, and Eu were analyzed. The U content was on average 4 ± 2 ppm, Th 8 ± 4 ppm, Se 1.5 ± 0.7 ppm, Cs 6 ± 3 ppm and Eu 1 ± 0.4 ppm which is comparable to other clay formations such as the Belgian and Dutch Boom Clay. All of these elements, except Se had high correlations with clay minerals. Looking at individual minerals, heavy minerals like rutile and zircon contained the highest content of the studied trace elements followed by clay minerals and feldspars. When taking into account the content of the minerals in the sediment, clay minerals were the most important fraction for all these trace elements, even though most of the analyzed samples were silty and sandy samples. For Se, also organic matter was a carrier. Carbonates, such as calcite, and pyrite did not play an important role in these sediments since they had a low trace elemental content and had a low abundancy in general.

These results contribute to an improved understanding and specifically to risk assessment of the fate of radionuclides in clay layers as host rock for radioactive waste. These mineral associations of natural analogues of radionuclides can be used for the prediction of retention of radionuclides in the long-term and can help to validate models on the radionuclide transport and retention used for radioactive waste disposal studies.

6 References

Adams, J. A., & Weaver, C. E. (1958). Thorium-to-uranium ratios as indicators of sedimentary processes: example of concept of geochemical facies. *AAPG Bulletin*, *42*(2), 387-430.

Balson, P. S. (1989). Tertiary phosphorites in the southern North Sea Basin: Origin, evolution and stratigraphic correlation.

Breynaert, E., Scheinost, A. C., Dom, D., Rossberg, A., Vancluysen, J., Gobechiya, E., ... & Maes, A. (2010). Reduction of Se (IV) in boom clay: XAS solid phase speciation. *Environmental science & technology*, *44*(17), 6649-6655.

Bruggeman, C., Salah, S., Maes, N., & Durce, D. (2017). Americium retention and migration behaviour in Boom Clay: Topical report–status 2015. *SCKCENER-0396. SCK• CEN Reports, https://researchportal. sckcen. be/en/publications/americium-retention-andmigration-behaviour-in-boom-clay-topical*.

Chisholm-Brause, C. J., Berg, J. M., Little, K. M., Matzner, R. A., & Morris, D. E. (2004). Uranyl sorption by smectites: spectroscopic assessment of thermodynamic modeling. *Journal of colloid and interface science*, *277*(2), 366-382.

DAPGEO-02 Multi-Purpose Research Borehole. https://www.tudelft.nl/citg/over-faculteit/afdelingen/geoscience-engineering/research/geothermal/geothermal-science-and-engineering/research/campus-geothermal-project/dapgeo-02-borehole

De Baar, H. J. W., Schijf, J., & Byrne, R. H. (1991). Solution chemistry of the rare earth elements in seawater. *European Journal of Solid State Inorganic Chemistry*, *28*.

De Cannière, P., Maes, A., Williams, S., Bruggeman, C., Beauwens, T., Maes, N. and Cowper, M., 2010. Behaviour of selenium in Boom Clay. *External Report, SCK• CEN-ER-120*.

De Craen, M., Delleuze, D., Volckaert, G., Sneyers, A., & Put, M. (2000). The Boom Clay as natural analogue. R-3444. Waste & Disposal Department, SCK•CEN, Mol, Belgium.

De Jong, T., Toshniwal, V., Broere, W., Vardon, P., Hicks, M., Dieudonne, A. (2024). SECUUR Progress Report Second Users Committee Meeting September 2024.

De Koning, A., & Comans, R. N. (2004). Reversibility of radiocaesium sorption on illite. *Geochimica et cosmochimica acta*, *68*(13), 2815-2823.

Durrant, C. B., Begg, J. D., Kersting, A. B., & Zavarin, M. (2018). Cesium sorption reversibility and kinetics on illite, montmorillonite, and kaolinite. *Science of the Total Environment*, *610*, 511-520.

De Meijer, R. J., van der Graaf, E. R., & Post, K. (2016). Radiometric properties of marine mammal fossils from the Westerschelde Estuary (Province of Zeeland, the Netherlands). *Deinsea*, *16*, 10-18.

Dooley, G.H. (2001). Baseline Concentrations of Arsenic, Beryllium and Associated Elements in Glauconite and Glauconitic Soils in the New Jersey Coastal Plain. Report by the New Jersey Department of Environmental Protection Division of Science, Research and Technology Geological Survey.

Dzombak, D. A., & Morel, F. M. (1990). *Surface complexation modeling: hydrous ferric oxide*. John Wiley & Sons.

Francis, C. W., & Brinkley, F. S. (1976). Preferential adsorption of 137Cs to micaceous minerals in contaminated freshwater sediment. *Nature*, *260*(5551), 511-513.

Fuller, A. J., Shaw, S., Ward, M. B., Haigh, S. J., Mosselmans, J. F. W., Peacock, C. L., ... & Burke, I. T. (2015). Caesium incorporation and retention in illite interlayers. *Applied Clay Science*, *108*, 128-134.

Giot R, Auvray C, Talandier J (2019) Self-sealing of claystone under X-ray nanotomography. Geol Soc London Special Publ 482(1):213–223. https://doi.org/10.1144/SP482.4

Gleyzes, C., Tellier, S., & Astruc, M. (2002). Fractionation studies of trace elements in contaminated soils and sediments: a review of sequential extraction procedures. *TrAC Trends in Analytical Chemistry*, *21*(6-7), 451-467.

Gustafsson, J. P., & Johnsson, L. (1992). Selenium retention in the organic matter of Swedish forest soils. *Journal of Soil Science*, *43*(3), 461-472.

Harsveldt, H. M. (1973). The discovery of uranium at Haamstede (Netherlands). In *New aspects of mineral and water resources in The Netherlands* (pp. 63-71). Dordrecht: Springer Netherlands.

Herr, S., Leybros, A., Barre, Y., Nikitenko, S., & Pflieger, R. (2022). Desorption of Cs from vermiculite by ultrasound assisted ion exchange. *Chemosphere*, *303*, 135175.

Hoving, A. L., Münch, M. A., Bruggeman, C., Banerjee, D., & Behrends, T. (2019). Kinetics of selenite interactions with Boom Clay: adsorption–reduction interplay.

Ithurbide, A. (2009). *Redox behaviour of uranium with iron compounds* (No. FRCEA-TH--2447). Universite Evry Val d'Essonne, 91-Evry (France).

Jacops, E., Maes, N., Bruggeman, C., & Grade, A. (2017). Measuring diffusion coefficients of dissolved He and Ar in three potential clay host formations: Boom Clay, Callovo-Oxfordian Clay and Opalinus Clay.

Koenen, M., & Griffioen, J. (2016). Characterisation of the geochemical heterogeneity of the Rupel Clay Member in the Netherlands. *Netherlands Journal of Geosciences*, *95*(3), 269-281.

Kuhlmann, G., 2004. High resolution stratigraphy and paleoenvironmental changes in the southern North Sea during the Neogene - An integrated study of Late Cenozoic marine deposits from the northern part of the Dutch offshore area. Ph.D. thesis, Utrecht University, Geologica Ultraiectina, Mededelingen van de Faculteit Aardwetenschappen 245: 205 pp

Loni, Y.H., David, K., Ribet, S., Lach, P., Lerouge, C., Madé, B., Bailly, C., Grambow, B. and Montavon, G., (2021). Investigation of europium retention on Callovo-Oxfordian clay rock (France) by laser ablation inductively coupled plasma mass spectrometry (LA-ICP-MS) and percolation experiments in microcells. *Applied Clay Science*, *214*, p.106280.

Ma, M., Behrends, T., expected in 2025. Determining the trace element composition in pore water of clay-rich sediments from the Paleocene and Eocene. Report.

Maes, N., Salah, S., Jacques, D., Aertsens, M., Van Gompel, M., De Canniere, P. and Velitchkova, N., 2008. Retention of Cs in Boom Clay: Comparison of data from batch sorption tests and diffusion experiments on intact clay cores. *Physics and Chemistry of the Earth, Parts A/B/C*, *33*, pp.S149-S155.

Missana, T., U. Alonso, and M. García-Gutiérrez. *Experimental Study and Modelling of the Sorption of Selenite and Europium Onto Smectite and Illite Clays*. No. CIEMAT--1171. Centro de Investigaciones Energeticas Medioambientales y Tecnologicas (CIEMAT), Madrid (Spain), 2009.

Montavon, G., Solange Ribet, Y. Hassan Loni, F. Maia, C. Bailly, Karine David, Catherine Lerouge, B. Madé, J. C. Robinet, and Bernd Grambow. (2022). Uranium retention in a Callovo-Oxfordian clay rock formation: From laboratory-based models to in natura conditions. *Chemosphere*, *299*, 134307.

Munsterman, D. (2023). *The results of the palynological analysis from core-shoe samples in borehole DAPGEO-02 (Delft), interval: 364.10-414.64 m* (tech. rep.). TNO. https://repository.tno.nl/islandora/object/uuid%3A1f4f372c-1edd-4338-8010-0c51c681cab2

Munsterman, D. K., Donders, T. H., Houben, A. J., Ten Veen, J. H., & Wesselingh, F. P. (2025). Paleogene–Neogene. *Geology of the Netherlands, second edition. Amsterdam University Press (Amsterdam)*, 293-331.

Nielsen, O. B., Rasmussen, E. S., & Thyberg, B. I. (2015). Distribution of clay minerals in the northern North Sea Basin during the Paleogene and Neogene: a result of source-area geology and sorting processes. *Journal of Sedimentary Research*, *85*(6), 562-581.

Oze, C., Smaill, J. B., Reid, C. M., & Palin, M. (2019). Potassium and Metal Release Related to Glaucony Dissolution in Soils. *Soil Systems*, *3*(4), 70. https://doi.org/10.3390/soilsystems3040070

Reiller, P., Moulin, V., Casanova, F., & Dautel, C. (2002). Retention behaviour of humic substances onto mineral surfaces and consequences upon thorium (IV) mobility: case of iron oxides. *Applied Geochemistry*, *17*(12), 1551-1562.

Schwertmann, U., Gasser, U., Sticher, H. (1989). Chromium-for-iron substitution in synthetic goethites, Geochimica et Cosmochimica Acta, Volume 53, Issue 6, Pages 1293-1297, ISSN 0016-7037

Séby, F., Potin-Gautier, M., Giffaut, E., & Donard, O. F. X. (1998). Assessing the speciation and the biogeochemical processes affecting the mobility of selenium from a geological repository of radioactive wastesto the biosphere. *Analusis*, *26*(5), 193-198.

Singer, D.M., Maher, K. and Brown Jr, G.E. (2009). Uranyl–chlorite sorption/desorption: Evaluation of different U (VI) sequestration processes. *Geochimica et Cosmochimica Acta*, *73*, pp.5989-6007.

Sharma, V. K., McDonald, T. J., Sohn, M., Anquandah, G. A., Pettine, M., & Zboril, R. (2015). Biogeochemistry of selenium. A review. *Environmental chemistry letters*, *13*(1), 49-58.

Stockdale, A., & Bryan, N. D. (2013). The influence of natural organic matter on radionuclide mobility under conditions relevant to cementitious disposal of radioactive wastes: A review of direct evidence. *Earth-Science Reviews*, *121*, 1-17.

Su, C., & Suarez, D. L. (2000). Selenate and selenite sorption on iron oxides an infrared and electrophoretic study. *Soil Science Society of America Journal*, *64*(1), 101-111.

Tischendorf, G., Förster, H. J., & Gottesmann, B. (2001). Minor-and trace-element composition of trioctahedral micas: a review. *Mineralogical Magazine*, *65*(2), 249-276.

Wang, K. (2022). *Reduction of Se (IV), Se (VI) and Re (VII) by Fe reactive phases present in CEMs and COx* (Doctoral dissertation, Université Grenoble Alpes [2020-....]).

Yong, R.N., Nakano, M., And Pusch, R. (2012). Environmental Soil Properties and Behaviour: London, CRC Press, 455 p

Zeelmaekers, E. (2011). Computerized qualitative and quantitative clay mineralogy: introduction and application to known geological cases. PhD Thesis. Katholieke Universiteit Leuven. Groep Wetenschap en Technologie: Heverlee. ISBN 978-90-8649-414-9. XII, 397 pp.

Zhang, Y., Wang, J., Qu, Y., Zhu, C., & Jin, Z. (2024). Mobility of rhenium and selenium during chemical weathering and their implication for petrogenic organic carbon oxidation. *Science China Earth Sciences*, *67*(3), 740-750.

Zhu, X. K., & O'Nions, R. K. (1999). Monazite chemical composition: some implications for monazite geochronology. *Contributions to Mineralogy and Petrology*, *137*(4), 351-363.

7 Signature

Author

ValidSigned by Alwina Hoving
on 2025-12-08 10:34:42

Dr. A.L. Hoving
Geochemist/Geomodeller

Second reader

ValidSigned by Joris Dijkstra
on 2025-12-04 12:03:50

Dr. J.J. Dijkstra
Senior Scientist Environmental Geochemistry

Authorisation release

ValidSigned by Yvonne Schavemaker
on 2025-12-04 12:36:58

Y.A. Schavemaker MSc
Research manager

8 Appendices

8.1 Appendix A - Core Shoe Description

Core sample	Shoe	Core Bottom Depth (m)	Core Top Depth (m)	Description	Core Description	Geological Formation
DAPGEO-02-C19	SH1	363.4	362.5	Grey clayey silt	very silty clay, mica, quite some forams/calcitic microfossils, few black mm-size specks, possibly ostracods	Diessen
DAPGEO-02-C20	SH2	364.1	363.4	Grey silty clay	silty clay, mica with golden shine, few forams, very few black specks, brown oxidation zones (from after coring)	Diessen
DAPGEO-02-C21	SH3	364.88	364.1	Grey silty clay	silty, sticky clay, some very fine mica, quite a lot of forams/calcitic microfossils in some laminae, some infauna and some benthics, some brownish oxidation zones (from after coring).	Diessen
DAPGEO-02-C24	SH4	366.71	365.9	Dark grey sandy clay	little darker grey, slicked, silty to sandy, sticky clay, white powdery recrystallized precipitate, sometimes in thin laminae mm-scale and some in shape of fossils, very few shiny forams, some very fine mica	Diessen
DAPGEO-02-C25	SH5	367.71	366.7	Dark grey/green sandy clay	dark green, grey sandy-silty clay, quite a lot of mica, very few forams, few slicks, white powdery mm-sized areas, recrystallized forams?	Diessen
DAPGEO-02-C26	SH6-2	368.51	367.7	Dark grey silty clay	silty, a bit micaceous clay, d. grey, some forams, some powdery fossil fragments, some fine, mm-scale slicks that do not seem from coring	Diessen
DAPGEO-02-C42	SH20	381.1	380.1	Grey/green very fine sandstone	mica-rich dark grey green, clayey very fine sandstone, few recrystalized spots, not very consolidated	Diessen
DAPGEO-02-C43	SH21	382.1	381.1	dark green/dark grey silt to very fine sandstone	mica-rich very fine sandstone, dark green, alternating with dark grey mica-rich coarse silt, few recrystallized white spots	Diessen
DAPGEO-02-C44	SH22	382.95	382.1	dark green, grey silty clay	very silty clay, some mica, very slicked throughout the rock, dark green, grey, some black grains?, very few recrystiled white spots	Diessen
DAPGEO-02-C48	SH25	386.05	385.2	very fine sandstone	mica-rich, very fine sandstone, dark grey green, homogeneous, possibly glauconitic	Grootte Heide

DAPGEO-02-C49	SH26	386.95	386.1	sandy silt	mica-rich, sandy silt, dark green grey, homogeneous	Grootte Heide
DAPGEO-02-C50	SH27	387.9	387	very fine sandstone to fine sandstone	shiny black round minerals, possibly glauconite, mica, quartz, homogeneous, poorly consolidated	Grootte Heide
DAPGEO-02-C51	SH28	388.85	387.9	very fine sandstone	glauconitic, very fine sandstone, dark green grey, mica-quartz, homogeneous, poorly consolidated	Grootte Heide
DAPGEO-02-C52	SH29	389.69	388.9	very fine sandstone to fine sandstone	very dark green-black,very fine sandstone to fine sandstone, shiny black round minerals, possibly glauconite or mica, nice round quartz, homogeneous, poorly consolidated, no fossils	Grootte Heide
DAPGEO-02-C53	SH30	390.69	389.7	very fine sandstone, glauconite	No fossils, no organic matter seen, a pyrite nodular concretion of 1 cm occurs, not seen in the shoe, it came on the side, homogeneous, not clayey: NOTE LATER: silt, 5GY 4/1 with 1cm diameter sand-filled burrow	Dongen (Ieper)
DAPGEO-02-C54	SH31	391.21	390.2	sandy silt	medium dark grey sandy silt, quartz, glauconite, some mica, homogeneous	Dongen (Ieper)
DAPGEO-02-C55	SH32	392.21	391.2	silt	dark greenish gray, 5GY 4/1, coarse silt, homogeneous	Dongen (Ieper)
DAPGEO-02-C57	SH33	393.66	392.7	silt and very fine sandstone	homogeneous, and clayey silt to silty clay, (mud), very dark grey, homogeneous	Dongen (Ieper)
DAPGEO-02-C62	SH34	397.75	396.9	very fine sandstone	very fine sandstone, dark olive gray 5Y 3/2, poorly consolidated, lamination of blackish stained and brown laminae, it seems small-scale cross bedding of these occur, glauconite, quartz, possibly some mica	Dongen (Oosteind)

8.2 Appendix B - Correlation Matrix - elements

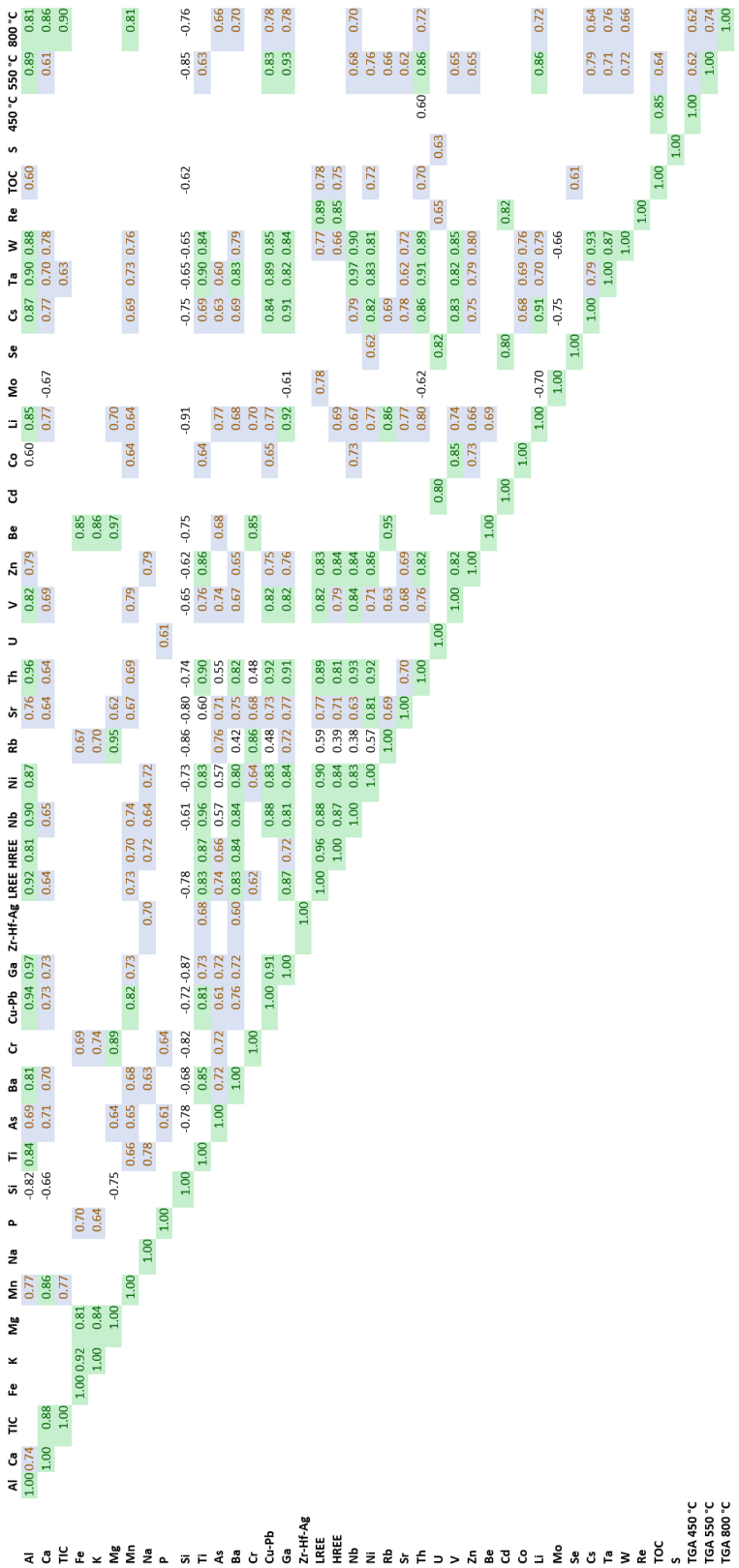

8.3 Appendix C - Correlation Matrix – minerals

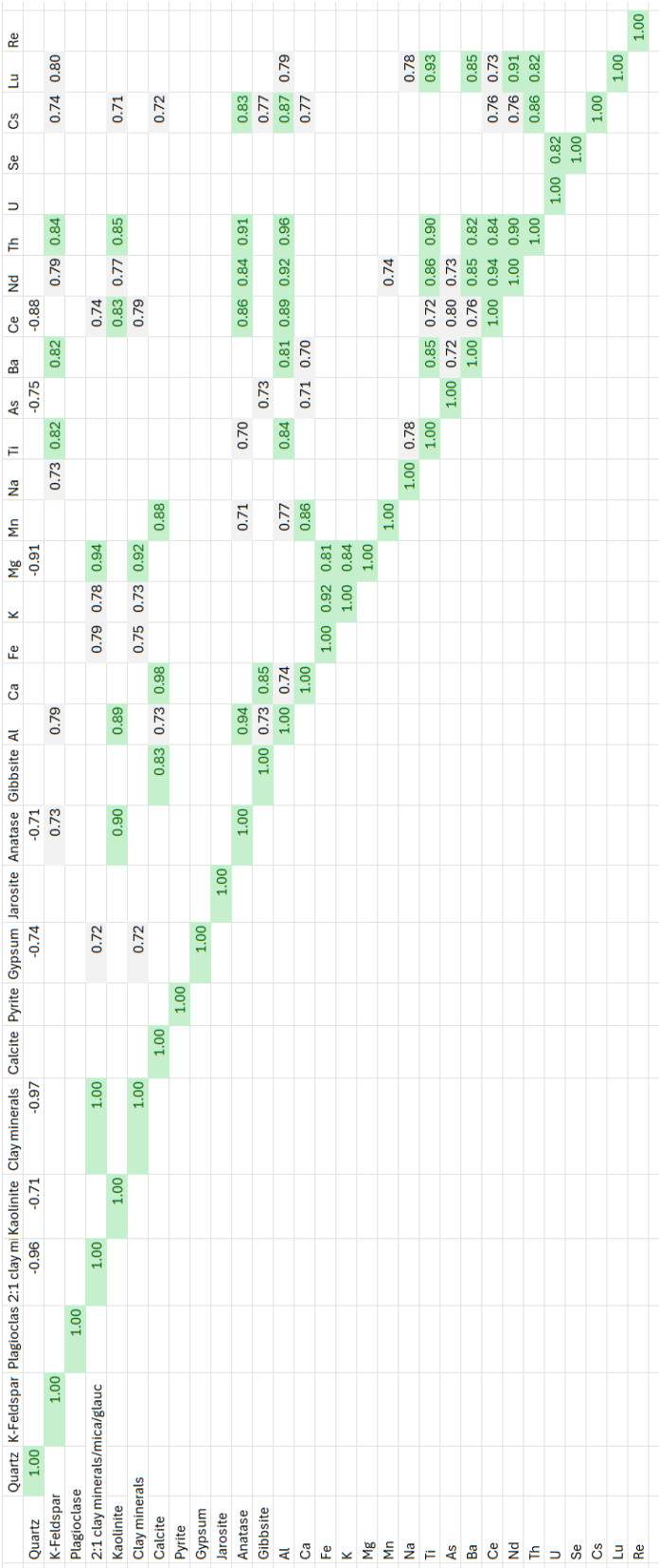

	Quartz	K-Feldspar	Plagioclas	2:1 clay mi	Kaolinite	Clay minerals	Calcite	Pyrite	Gypsum	Jarosite	Anatase	Gibbsite	Al	Ca	Fe	K	Mg	Mn	Na	Ti	As	Ba	Ce	Nd	Th	U	Se	Cs	Lu	Re
Quartz	1.00			-0.96	-0.71	-0.97			-0.74		-0.71						-0.91				-0.75		-0.88							
K-Feldspar		1.00									0.73		0.79						0.73	0.82		0.82		0.79	0.84			0.74	0.80	
Plagioclase			1.00																											
2:1 clay minerals/mica/glauc				1.00		1.00			0.72				0.89		0.79	0.78	0.94						0.74					0.71		
Kaolinite					1.00						0.90												0.83	0.77	0.85					
Clay minerals						1.00			0.72						0.75	0.73	0.92						0.79							
Calcite							1.00					0.83	0.73	0.98				0.88										0.72		
Pyrite								1.00																						
Gypsum									1.00																					
Jarosite										1.00																				
Anatase											1.00		0.94					0.71		0.70			0.86	0.84	0.91			0.83		
Gibbsite												1.00	0.73	0.85							0.73							0.77		
Al													1.00	0.74				0.77		0.84		0.81	0.89	0.92	0.96			0.87	0.79	
Ca														1.00				0.86			0.71	0.70						0.77		
Fe															1.00	0.92	0.81													
K																1.00	0.84													
Mg																	1.00													
Mn																		1.00						0.74						
Na																			1.00	0.78									0.78	
Ti																				1.00		0.85	0.72	0.86	0.90				0.93	
As																					1.00	0.72	0.80	0.73						
Ba																						1.00	0.76	0.85	0.82				0.85	
Ce																							1.00	0.94	0.84			0.76	0.73	
Nd																								1.00	0.90			0.76	0.91	
Th																									1.00			0.86	0.82	
U																										1.00	0.82			
Se																											1.00			
Cs																												1.00		
Lu																													1.00	
Re																														1.00

8.4 Appendix D- XRF data

		wt%	wt%	wt%	wt%	wt%	wt%	mg/kg	wt%	wt%	wt%	wt%
Depth (m)	Sample code	Al	Ca	TIC	Fe	K	Mg	Mn	Na	P	Si	Ti
363.4	C19	9.98	3.28	0.64	3.39	2.52	1.1	311.51	0.7	0.05	24.04	0.55
364.1	C20	9.6	3.53	0.54	6.61	2.34	1.24	578.03	0.71	0.1	21.72	0.5
364.88	C21	10.78	2.63	0.22	4.24	2.6	1.17	367.7	0.8	0.06	23.45	0.52
366.71	C24	7.88	1.81	0.02	3.93	2.72	1.41	203.69	0.92	0.07	25.25	0.49
367.71	C25	7.62	1.29	0	4.45	2.78	1.44	221.37	0.98	0.05	26.58	0.51
368.51	C26	8.05	1.87	0.07	4.39	2.77	1.44	226.04	0.97	0.06	26.82	0.48
381.1	C42	5.07	0.31	0	3.8	2.38	0.91	116.71	0.9	0.03	32.58	0.43
382.1	C43	5.75	0.28	0	3.78	2.22	0.83	94.11	0.8	0.03	27.63	0.42
382.95	C44	9.53	0.09	0	4.16	2.09	1.07	149.75	0.88	0.03	24.71	0.54
386.05	C48	5.21	0.56	0	7.75	3.72	1.4	99.95	0.92	0.17	27.52	0.31
387.9	C50	4.07	0.25	0	8.77	4.35	1.44	80.92	0.58	0.09	29.12	0.13
388.85	C51	3.44	0.44	0	8.52	4.51	1.57	74.13	0.61	0.08	29.28	0.21
389.69	C52	2.94	0.25	0	8.63	4.41	1.49	72	0.6	0.07	30.34	0.18
390.69	C53	5.28	0.36	0	2.92	2.52	0.78	229.04	1.02	0.08	33.69	0.54
391.21	C54	3.42	0.24	0	1.62	1.79	0.39	155.06	0.89	0.04	38.23	0.39
392.21	C55	5.13	0.22	0	2.39	1.88	0.68	158.05	0.79	0.04	37.05	0.38
393.66	C57	7.52	0.4	0	4.11	2.76	1.29	223.19	0.97	0.05	29.78	0.44
397.75	C62	0.73	0.03	0	0.5	0.38	0.08	13.46	0.33	0	43.71	0.03
406.11	C75	5.6	2.98	na	2.59	1.92	0.92	0.01	1.86	0.03	29.68	0.54

mg/kg	mg/kg	mg/kg	mg/kg	mg/kg	mg/kg	mg/kg	mg/kg	mg/kg	mg/kg	mg/kg	mg/kg	mg/kg	mg/kg	mg/kg	mg/kg	mg/kg	mg/kg	mg/kg	mg/kg	mg/kg	mg/kg	mg/kg	mg/kg
As	Ba	Ce	Cr	Cu	Ga	Hf	La	Nb	Nd	Ni	Pb	Pr	Rb	Sc	Sn	Sr	Th	U	V	Y	Zn	Zr	Rh
31.55	438.44	98.09	127.07	28.59	22	3.2	45.57	31.86	37.42	50.75	26	10.04	131.92	19.51	4.9	420.59	12.29	3.01	164.41	20.39	86.19	113.75	32
28.56	395.46	96.68	120.1	39.37	24	2.82	42.85	26.14	35.74	47.65	28	9.57	128.68	19.87	3.5	609.21	11.82	2.94	175.45	19.94	84.98	100.53	26
32.32	405.68	98.06	128.6	29.6	26	2.94	43.4	26.78	35.87	51.81	30	9.66	140.65	20.29	3.98	481.31	12.84	3.15	173.74	19.71	88.23	103.94	28
26.39	369.57	83.44	136.1	24.71	21	2.79	35.04	24.76	29.67	54.23	21	7.93	149.44	18.76	3.3	510.06	11.48	3.3	170.62	16.37	97.14	96.14	31
24.78	351.48	80.14	139.11	22.11	21	2.95	32.49	24.44	27.55	52.48	22	7.38	144.8	19.17	3.26	484.14	10.84	3.58	162.91	15.41	101.86	102.08	30
19.26	348.67	78.97	138.28	21.1	18	2.94	31.77	22.35	27.04	52.2	19	7.29	143	18.06	3.78	501.64	10.64	3.95	149.98	14.66	98.5	100.44	31
12.75	322.35	66.62	113.63	18.98	8	5.4	27.41	18	24.56	43.8	8	6.54	78.91	11.51	2.73	376.07	8.19	4.94	73.11	13.52	67.84	216.17	33
14.45	334.87	57.77	108.01	16.58	11	4.65	23.85	17.79	20.24	32.17	11	5.47	78.5	11.04	5.09	398.86	7.66	4.18	67.95	11.07	61.94	185.17	33
17.18	315.65	101.01	139.34	31.47	24	3.28	40.91	25.08	34.6	60.67	24	9.39	114.95	19.7	3.1	369.71	14.27	5.7	117.94	17.19	103.83	110.66	32
28.03	395.46	84.66	169.62	17.26	12	3.21	28.67	12.64	28.97	52.02	10	7.37	121.02	13.04	1.8	542.77	6.76	11.15	81.5	23.23	70.31	105.71	27
23.42	189.26	59.88	131.84	4.42	11	1.39	15.59	5.39	15.68	15.63	8	4.11	134.81	8.56	0.92	333.24	2.28	4.16	94.33	6.8	51.39	45.82	26
19	214.72	62.42	131.49	7.51	9	1.68	18.24	11.06	17.26	23.49	7	4.54	133.93	10.43	1.69	297.58	3.7	3.45	88.09	9.25	61.22	56.44	25
20.32	229.25	68.17	132.58	5.75	7	1.75	19.58	7.76	18.31	18.43	5	4.82	135.62	9.23	1.87	313.29	3.66	3.87	85.32	9.51	55.57	59.78	25
23.12	328.38	67.97	106.96	17.12	9	4.1	30.2	22.81	27.86	34.5	11	7.14	72.88	13.2	2.35	353.19	7.21	5.18	132.26	21.69	106.16	171.45	34
15.6	306.84	42.45	80.38	12.81	5	3.41	20.41	16.13	19.61	20.08	9	5.06	47.88	8.47	1.17	194.43	5.21	4.51	114.15	14.11	51.75	138.08	37
16.09	276.8	59.32	79.22	17.36	10	2.96	27.13	20.13	23.31	30.6	11	6.09	71.53	11.89	1.4	361.02	6.39	3.84	114.92	16.55	73.79	120.01	36
19.91	284.56	87.14	117.94	31.6	17	2.8	39.3	23.59	34.92	54.99	19	9.12	121.27	20.09	11.38	480.14	9.23	6.67	177.21	21.7	105.99	104.63	31
2.74	131.59	10.47	13.55	3.79	0	0.4	4.95	2.08	4.32	4.19	1	1.14	14.51	1.18	2.88	157.7	1.01	1.62	11.34	2.6	21.04	14.16	41
2.3	657.39	57.67	112.63	22.55	11.27	8.78	29.65	12.8	28.92	39.65	11.27	7.6	64.93	21.46	0.95	1098.72	6.89	1.84	92.21	29.33	93.12	223.13	33.27

mg/kg	mg/kg	mg/kg	mg/kg	mg/kg	mg/kg	mg/kg	ug/kg	mg/kg	mg/kg	mg/kg	mg/kg	mg/kg	mg/kg	mg/kg	mg/kg	mg/kg	mg/kg	mg/kg	mg/kg	mg/kg	mg/kg	mg/kg	ug/kg	ug/kg	mg/kg	wt%	wt%
Be	Cd	Co	Li	Mo	Se	Ag	In-IS	Sb	Cs	Sm	Eu	Gd	Tb	Dy	Ho	Er	Tm	Yb	Lu	Ta	W	Re	Hg	Tl	TOC	S
2.71	0.16	16.9	100.74	1.2	1.24	0.33	1.01	1.35	9.08	7.03	1.53	5.88	0.79	4.35	0.81	2.33	0.32	2.12	0.31	2.65	2.22	3.57	75.35	1.13	1.1	0.39
2.8	0.16	15.65	103.47	1.56	1.3	0.3	1	1.05	9.24	6.72	1.48	5.63	0.76	4.19	0.79	2.26	0.32	2.05	0.3	1.89	2.1	4.66	48.96	0.83	1.36	0.35
2.79	0.14	16.42	115.64	1.2	1.26	0.31	1.01	1.08	9.84	6.63	1.43	5.55	0.75	4.17	0.78	2.26	0.31	2.07	0.31	1.87	2.15	3.42	34.15	0.74	1.33	0.38
2.93	0.19	16.63	106.25	1.16	1.25	0.29	1	0.86	10.61	5.52	1.14	4.62	0.62	3.47	0.65	1.92	0.27	1.78	0.26	1.74	2.14	6.64	25.49	0.66	1.76	0.79
2.86	0.19	17.39	99.09	1.58	1.33	0.29	1.02	0.83	10.24	5.14	1.08	4.26	0.58	3.23	0.62	1.81	0.26	1.73	0.26	1.64	2.06	7.53	16.31	0.62	1.59	1.1
2.79	0.21	17.72	91.3	1.41	1.23	0.28	1.01	0.87	9.78	5.08	1.04	4.17	0.56	3.09	0.58	1.72	0.24	1.62	0.24	1.49	2.58	11.65	75.39	0.6	1.64	1.39
1.83	0.37	4.48	52.98	5.7	2.25	0.49	1.07	0.99	4.11	4.6	0.82	3.78	0.49	2.67	0.5	1.49	0.22	1.51	0.23	1.25	0.95	20.17	-7.27	0.41	2.03	1.04
1.73	0.28	3.82	48.51	11.32	1.85	0.43	1.03	0.84	3.95	3.72	0.72	3.06	0.4	2.2	0.42	1.26	0.19	1.31	0.2	1.24	0.85	17.88	-14.93	0.33	2.04	1.38
2.35	0.27	8.13	89.97	5.47	2.61	0.31	0.99	1.18	7.19	6.33	1.39	5.15	0.68	3.73	0.69	2	0.28	1.87	0.28	1.8	1.43	17.93	-4.15	0.39	2.14	2.52
3.01	0.49	5.06	68.78	8.03	3.21	0.32	1.01	1.7	4.82	5.96	1.28	5.23	0.72	3.98	0.76	2.15	0.28	1.76	0.26	0.98	0.69	34.58	-1.02	0.58	1.38	2.04
3.5	0.3	4.84	52.52	19.2	0.84	0.16	0.98	1.44	2.83	2.94	0.63	2.33	0.28	1.39	0.24	0.66	0.09	0.54	0.08	0.38	0.15	35.07	-31.69	0.28	0.61	0.95
3.5	0.12	4.89	73.27	7.64	1.05	0.2	1.06	1.53	4.09	3.26	0.7	2.71	0.34	1.8	0.32	0.9	0.12	0.76	0.11	0.87	0.45	10.07	81.96	1.47	0.44	0.8
3.31	0.18	4.43	61.16	12.09	0.98	0.19	1	1.38	3.5	3.45	0.71	2.86	0.36	1.86	0.33	0.9	0.12	0.75	0.11	0.52	0.24	15.87	33.43	0.74	0.35	2.12
1.46	0.25	17.67	41.61	18.93	1.52	0.39	1.07	0.81	3.89	5.56	1.23	5	0.71	4.14	0.81	2.36	0.34	2.2	0.33	1.44	1.28	20.62	29.64	0.56	0.42	2.44
1.04	0.15	11.32	22.36	15.91	0.87	0.33	1.11	0.58	2.14	3.94	0.84	3.45	0.48	2.75	0.52	1.51	0.22	1.44	0.22	1.1	0.75	15.61	8.25	0.39	0.18	0.97
1.67	0.2	15.47	39.44	9.24	1.23	0.32	1.07	0.48	4.29	4.49	1	3.95	0.55	3.15	0.61	1.81	0.25	1.69	0.25	1.11	0.97	4.32	2.75	0.35	0.39	0.85
2.78	0.2	24.08	63.78	12.55	1.66	0.3	1.14	1.05	7.7	6.76	1.46	5.72	0.77	4.3	0.82	2.36	0.33	2.13	0.31	1.86	1.46	5.31	24.78	0.45	0.85	1.65
0.29	0.13	6.37	12.64	5.27	0.33	0.08	1.08	0.32	2.31	0.83	0.19	0.72	0.09	0.49	0.09	0.29	0.04	0.26	0.04	0.19	0.06	1.96	2.84	0.2	0.4	0.47
na	na	na	na	na	na	na	na	na	na	na	na	na	na	na	na	na	na	na	na	na	na	na	na	na	0.32	0.39

8.5 Appendix E – XRD – Bulk

			Feldspars		Clay minerals		Carbonates				Ti-oxides				Secondary minerals	
	Depth (m)	Quartz	K-Feldspar	Plagioclase	2:1 clay minerals/mica/glauconite	Kaolinite	Calcite	Ankerite	Siderite	Pyrite	Rutile	Anatase	Gibbsite	Clinoptilolite	Gypsum	Jarosite
DAP-C19	363.4	25.6	2.3	4.7	46.2	6.6	7.5	0.8	<0.5	<0.5	<0.5	1.7	1.4	<0.5	3	<0.5
DAP-C20	364.1	23.5	2.4	3	47.2	5.3	9.1	1	1.6	<0.5	<0.5	2.2	0.8	<0.5	3.3	<0.5
DAP-C21	364.88	22.2	2.7	2.9	52.4	6.2	6.4	0.9	<0.5	0.7	<0.5	1.9	1.1	<0.5	1.8	0.5
DAP-C24	366.71	23.2	2.4	4.6	51.7	3.9	3.4	4.1	<0.5	1.2	<0.5	1.6	0.7	<0.5	2.7	<0.5
DAP-C25	367.71	25.1	2.5	4.6	50.6	3.3	2.2	4.8	<0.5	1.4	<0.5	1.4	0.8	<0.5	2.5	0.8
DAP-C26	368.51	25.1	2.7	5.3	51	3.3	3.7	2.5	<0.5	1.4	<0.5	1.4	<0.5	<0.5	2.1	0.9
DAP-C42	381.1	45.1	2.8	5	40.7	2.7	0.6	<0.5	<0.5	0.6	<0.5	1	<0.5	<0.5	0.6	<0.5
DAP-C43	382.1	45.5	1.6	4.7	39.6	3.2	0.7	<0.5	<0.5	<0.5	<0.5	1	<0.5	<0.5	1	2.2
DAP-C44	382.95	18	2.2	4.6	59.2	7.1	0.6	<0.5	<0.5	1.3	<0.5	2.2	<0.5	<0.5	3.1	1.3
DAP-C48	386.05	23.8	2.2	4.9	57.6	2.6	<0.5	<0.5	<0.5	<0.5	<0.5	1.1	<0.5	<0.5	5.2	1.9
DAP-C50	387.9	25.4	1	2	60.8	2.5	<0.5	<0.5	<0.5	0.8	<0.5	0.8	<0.5	<0.5	4	1.7
DAP-C51	388.85	29	0.8	3.3	56.3	2.4	1.3	<0.5	<0.5	<0.5	<0.5	0.6	<0.5	<0.5	2.4	3.1
DAP-C52	389.69	31.2	0.5	3.7	57.9	1.8	0.7	<0.5	<0.5	0.9	<0.5	<0.5	0.5	<0.5	1.7	0.6
DAP-C53	390.69	53.4	1.8	10.6	27.5	1.6	<0.5	<0.5	<0.5	0.9	<0.5	0.6	<0.5	<0.5	1.7	1.4
DAP-C54	391.21	71.6	1.6	7.6	15	1	0.6	<0.5	<0.5	<0.5	<0.5	<0.5	<0.5	<0.5	0.8	<0.5
DAP-C55	392.21	56.4	1.1	7.6	29.3	1.2	0.7	<0.5	<0.5	<0.5	<0.5	0.9	<0.5	<0.5	0.6	1.3
DAP-C57	393.66	31	2.4	4.2	51.9	2.6	0.8	<0.5	<0.5	2.1	<0.5	1.3	0.6	<0.5	2	0.9
DAP-C62	397.75	92.8	0.6	0.9	4.2	<0.5	<0.5	<0.5	<0.5	<0.5	<0.5	<0.5	<0.5	0.8	<0.5	<0.5
DAP-C75	406.11	26.9	2.6	5.7	32.2	0.9	8.3	<0.5	<0.5	1	<0.5	<0.5	<0.5	19.7	<0.5	<0.5

8.6 Appendix F – XRD clay fraction

	Depth (m)	Chlorite (wt%)	Total smectitic content (wt%)	Total illitic content (wt%)	Total Kaolinite (wt%)
DAP-C19	363.4	2.2	43.7	28.9	17.4
DAP-C20	364.1	1.9	36.3	37.4	16.3
DAP-C21	364.88	2.2	35.3	37.2	16.7
DAP-C24	366.71	2.9	44.5	32.9	14
DAP-C25	367.71	1.5	45.5	42.3	8.5
DAP-C26	368.51	1.3	49.4	40.3	7.8
DAP-C42	381.1	0.3	51.7	28.2	14.8
DAP-C43	382.1	0.1	47.5	29	16.7
DAP-C44	382.95	0.1	48.9	9.7	28.5
DAP-C48	386.05	0	51.5	30.2	13.8
DAP-C50	387.9	0.1	56.6	24.6	14.4
DAP-C51	388.85	0.1	65.5	15.9	15.4
DAP-C52	389.69	0	62	30.6	8
DAP-C53	390.69	1	70.7	25.7	5.7
DAP-C54	391.21	0.4	68.5	29.6	5
DAP-C55	392.21	0.3	66.9	33.8	3.1
DAP-C57	393.66	0.4	68.8	32.9	2.6
DAP-C62	397.75	0	78.6	19.1	6.1
DAP-C75	406.11	0.2	83.66	16.14	0

Clay mineral composition of the <2 µm size fraction. Smectitic content refers to the sum of smectite and smectitic layers in interstratified illite/smectite (I-S), and the illitic content refers to the sum of illite and illitic layers in interstratified illite/smectite (I-S).

Energy & Materials Transition

Princetonlaan 6
3584 CB Utrecht
www.tno.nl

TNO innovation for life